BULETINUL INSTITUTULUI POLITEHNIC DIN IAŞI

Volumul 62 (66)
Numărul 2

Secţia
CONSTRUCŢII DE MAŞINI

2016 **Editura POLITEHNIUM**

BULETINUL INSTITUTULUI POLITEHNIC DIN IAŞI
PUBLISHED BY
"GHEORGHE ASACHI" TECHNICAL UNIVERSITY OF IAŞI
Editorial Office: Bd. D. Mangeron 63, 700050, Iaşi, ROMANIA
Tel. 40-232-278683; Fax: 40-232-237666; *e-mail*: polytech@mail.tuiasi.ro

BULETINUL INSTITUTULUI POLITEHNIC DIN IAŞI
BULLETIN OF THE POLYTECHNIC INSTITUTE OF IAŞI
Volumul 62 (66), Numărul 2 2016

Secția

CONSTRUCŢII DE MAŞINI

SUMAR

B U L E T I N U L   I N S T I T U T U L U I   P O L I T E H N I C   D I N   I A Ş I
B U L L E T I N O F T H E P O L Y T E C H N I C I N S T I T U T E O F I A Ş I
Volume 62 (66), Number 2 2016

Section

MACHINE CONSTRUCTION

C O N T E N T S

BULETINUL INSTITUTULUI POLITEHNIC DIN IAŞI
Publicat de
Universitatea Tehnică „Gheorghe Asachi” din Iaşi
Volumul 62 (66), Numărul 2, 2016
Secţia
CONSTRUCŢII DE MAŞINI

INFLUENCE OF THE PATTERNED SURFACES ON THE FLOW SPECTRUM AROUND THE IMMERSED BODIES

BY

NICOLETA OCTAVIA TĂNASE* and DIANA BROBOANĂ

University “Politehnica” of Bucureşti,
Power Engineering Faculty

Received: April 26, 2016
Accepted for publication: November 29, 2016

Abstract. The paper is dedicated to the experimental and numerical studies of the free surface flows around immersed bodies (a cylinder and a broad – crested weir) with smooth and patterned surface. The study analyses the qualitative differences between the smooth and patterned surfaces of the immersed bodies, as function of the immersed depths for weakly turbulent flows ($Re < 10^4$) in subcritical regimes ($Fr < 1$). The results indicate that presence of a grooved geometry with small aspect ratio on the surface of the bodies changes the flow spectrum in the vicinity and downstream the separation of the shear layers.

Keywords: immersed cylinders; broad – crested weir; visualizations flow; numerical simulations; grooved geometry.

1. Introduction

The dynamics of the flow around immersed bodies in a channel with free surface is an important topic of study in hydrology, hydraulics, in the design of water turbines plant, marine platforms and inflatable dams. The characterization of the flow over the immersed bodies becomes recently a

*Corresponding author; *e-mail*: octavia.tanase@upb.ro

subject of interest also for some other domains of fluid mechanics as microfluidics and complex flows in presence of microstructures (Sheridan *et al*., 1995; Lee and Daichin, 2004; Rahimzadeh *et al*., 2012; Chamorro *et al*., 2013).

The flow is characterized by the non-dimensional Reynolds, respectively Froude numbers:

$$Re = \frac{\rho L \mathrm{V}_0}{\eta}, \; Fr = \frac{\mathrm{V}_0}{\sqrt{g L}}. \tag{1}$$

where $\rho = 1000$ kg/m^3 is mass density, $\eta = 1$ mPas is the viscosity, V_0 is the average velocity upstream the broad - crested weir, g is the gravitational acceleration and L is the space scale ($L \equiv D$, D is the cylinder diameter, respectively L is the length of broad-crested weir).

The flow takes place in subcritical weakly turbulent regime, characterized by the Froude number less than one and Reynolds number less than 10^4. Numerical simulations are performed with the turbulent solvers implemented in FLUENT, using the VOF code for the calculation of the free surface geometry. The numerical results and the visualizations are corroborated to determine the influence of micro - geometries, especially in the region between the free surface and the separation point. The evolution of the wake downstream the bodies and the onset of Kelvin-Helmholtz instabilities are also investigated for the smooth and grooved geometries.

The experimental investigations were focused to the region between the free surface and the domain downstream the bodies. The positions of the upper and lower separation points of the boundary layer from the cylinder and the wake trace were the main experimental characteristics compared with the numerical results.

2. Experimental Set-up

The experiments are performed in a free surface transparent water channel, which is connected to a constant level water supply tank. The flow rate and the fluid height upstream the body are controlled by a weir. The average velocity V_0 is computed (from the measured flow rate) for the upstream area for the height H_0 which is maintained constant. The bodies are located at the distance 303 mm from the entrance section, for details see (Tănase, 2013; Tănase *et al*., 2014a; Tănase *et al*., 2014b; Tănase *et al*., 2015).

The dimensions of the broad – crested weir are: $L = 70$ mm, height 35 mm and the cylinder diameter is $D = 50$ mm. Visualizations of free surface flow and the measurements are performed at different constant entrance water levels H_0 and the constant height of the weir h_w, Fig. 1.

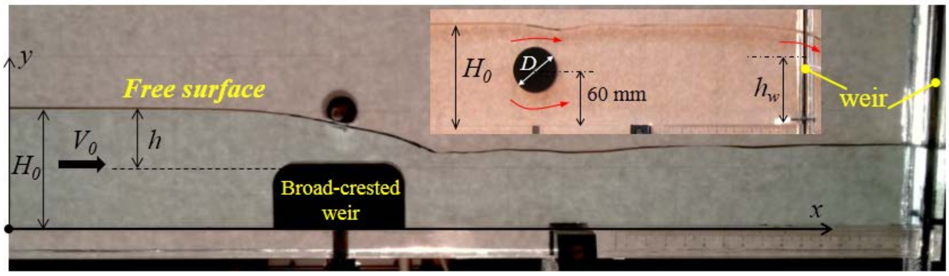

Fig. 1 – The geometry of the experimental channel of 15 mm width, cylinder diameter D = 50 mm and length broad-crested weir of L = 70 mm.

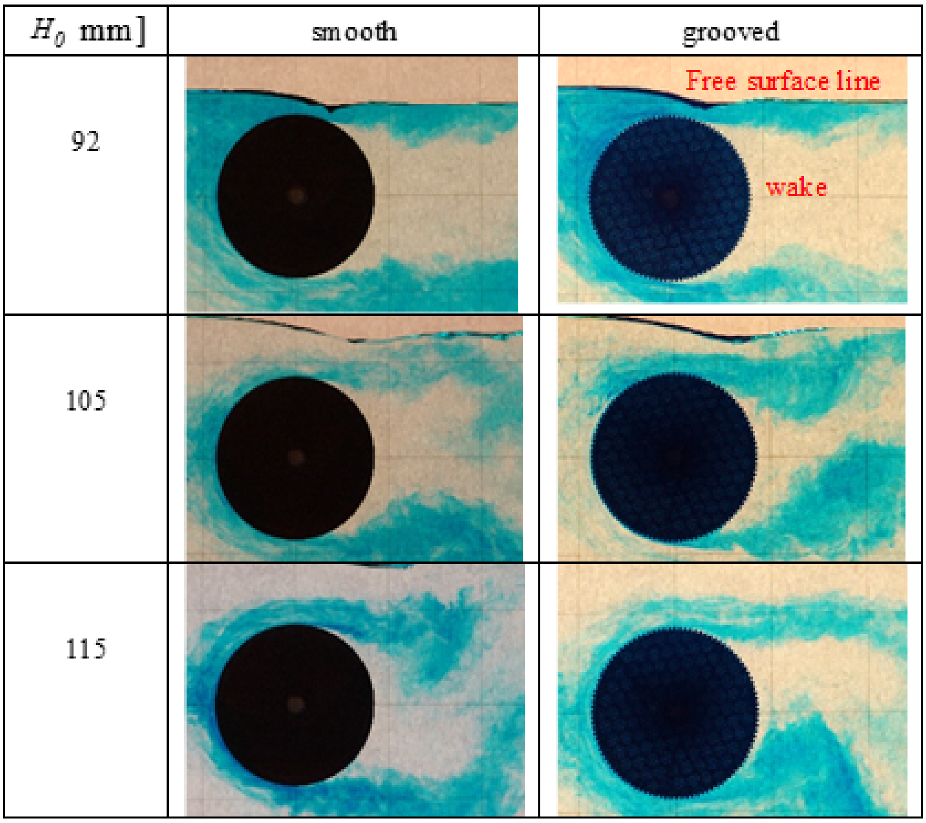

Fig. 2 – Flow visualizations around immersed smooth and grooved cylinders at different immersed depths H_0.

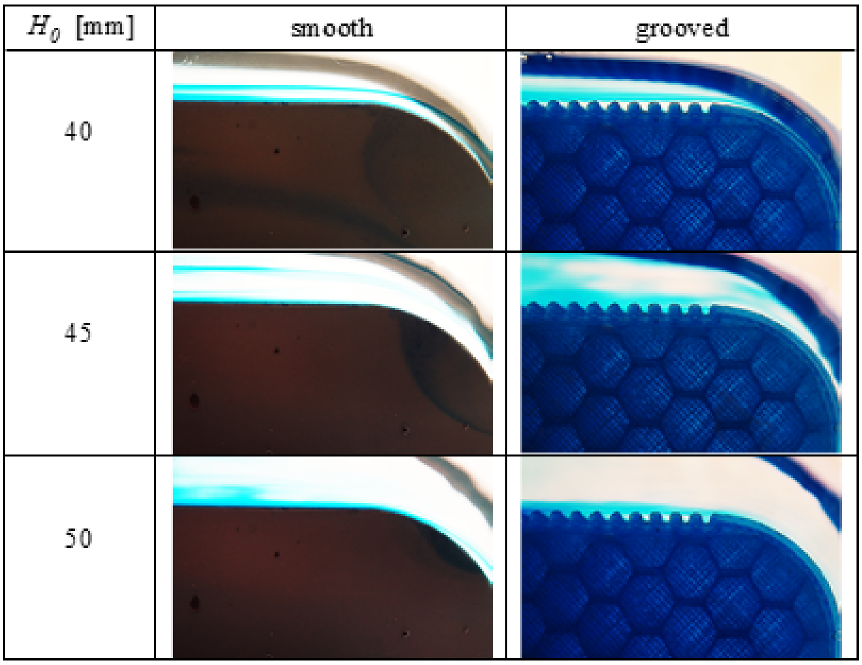

Fig. 3 – Flow visualization of the smooth and grooved surfaces of the broad - crested weir at different immersed depths H_0 .

A color dye was introduced upstream the immersed obstacle and the direct visualization of the streak lines is obtained using a performed SONY digital camera at a rate of 12 images/s, see Figs. 2 and 3. Macro lens and high resolution up to 25 MP are used to take picture of the flow in vicinity of the bodies with grooved surfaces (which were fabricated by the 3D printing technology).

3. Numerical Simulations

The free surface flow around cylinders and weirs (smooth and grooved surfaces) were investigated also numerically at constant height H_0 ($H_0 = 105$ mm for cylinders and $H_0 = 50$ mm for weirs, which corresponding to the velocity $V_0 = 0.15$ m/s, respectively $V_0 = 0.05$ m/s). Simulations are performed in a 2D and 3D geometry of the channel using structured mesh, see Table 1 and Fig. 4. All dimensions from the experiments are identical to both 2D and 3D numerical simulations ($D = 50$ mm, $L = 70$ mm). The turbulence model used for the numerical simulations of free surface flow around an immersed smooth cylinder was k - ε RNG (options Differential Viscosity

Model) with the VOF method to compute the free surface (Launder and Spalding, 1972; Broboană *et al*., 2007; Fluent Inc., 2008).

The entrance boundary condition is linear pressure distribution $p = \rho g y$, $0 \le y \le H_0$, with the exit constant atmospheric pressure imposed, $p = p_0$ and the adherence conditions on the cylinder/weir and the lower wall: $\mathbf{v} = 0$ (Tănase *et al*., 2014b). The flows are considered steady; no influence of surface tension was analyzed in these cases.

The numerical simulation are performed on a 64-bit server Dual 2.33 GHz with 16 GB RAM memory, the computation time for each 2D case being around 2 days and for 3D case around 4 days, for a precision of 10^{-5}.

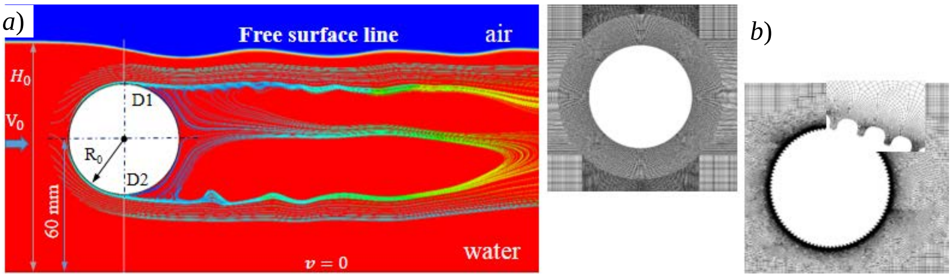

Fig. 4 – *a*) Numerical working domain, initial phases configurations, *b*) structured mesh in vicinity of the cylinder. Similar qualitatively meshes are used of the simulations around the weirs.

Table 1
The Mesh Characteristics of the 3D in Comparison with the 2D

Case	Cells	Faces	Nodes
3D cylinder	2.298.888	7.118.685	2.522.435
2D cylinder	638.436	1.270.606	632.170

The obtained 3D solutions are stable but the comparison with experiments doesn’t emphasis a better fitting and representation of experiments than the 2D case, see Figs. 5 and 6. This result is consistent with the experimental conditions and observations: the width of the flow channel is relatively small in comparison to the other dimensions, so the parallel lateral walls induce a pseudo-planar motion in the region where the body is located. On the other hand, the performed 3D simulations are limited by the available computations machines on the number of nodes, so it we expect a lower precision of the computations.

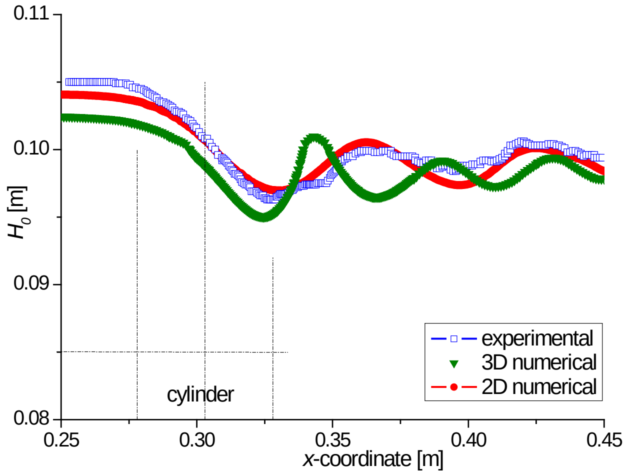

Fig. 5 – Comparison of the average measured experimental free surface with the 2D and 3D steady solutions.

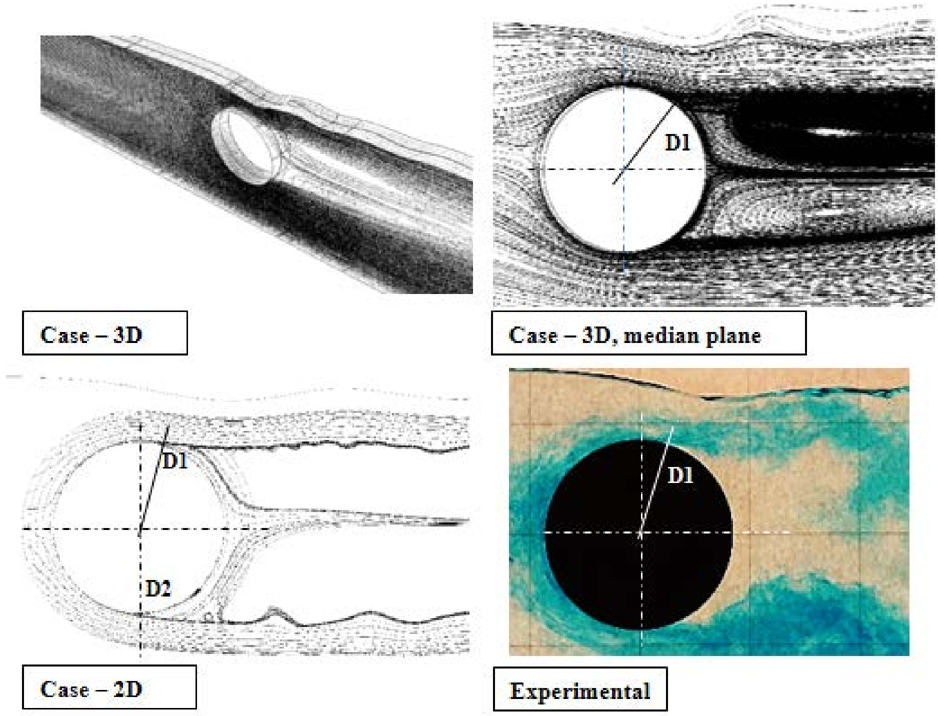

Fig. 6 – Flow spectrum in the 3D and 2D computations. It is observed that separation point D1 is located for the 3D solution at larger angle than for 2D case (which gives almost the same value as in experiments), $\theta_{2D} = 106°$, $\theta_{3D} = 110°$, $\theta_{\exp} = 107°$.

The analysis of the numerical results (free surface profile, location of separation points, wake structure) in relation to the experiments visualization concludes that 2D geometry is more indicated to simulate the flow under investigation.

The numerical spectrum is computed (for the same geometry and flow conditions) and the results are compared and calibrated with the experimental flow patterns, for both smooth and grooved geometries.

The computed free surface lines are compared with the experimental free surface line in Fig. 7. One can be noticed that experimental free surface line upstream of the cylinder is perfectly reproduced numerically, for details see (Tănase *et al*., 2014b).

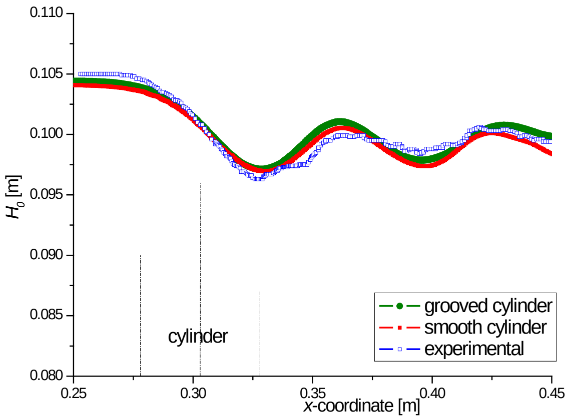

a)

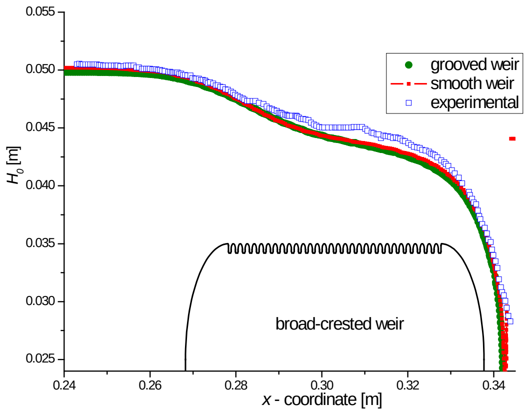

b)

Fig. 7 – Comparison of the experimental free surface line with the numerical solutions for the both surfaces of the bodies: (*a*) cylinders and (*b*) weirs.

The free surface lines in the vicinity of the immersed bodies are almost identical for both types of surfaces, but qualitative differences in formation of Kelvin-Helmholtz instabilities are observed between smooth and grooved surfaces, Fig. 8. The patterned surface influences also the separation point position and consequently the drag force acting on the immersed bodies, (El-Makdah and Oweis, 2013).

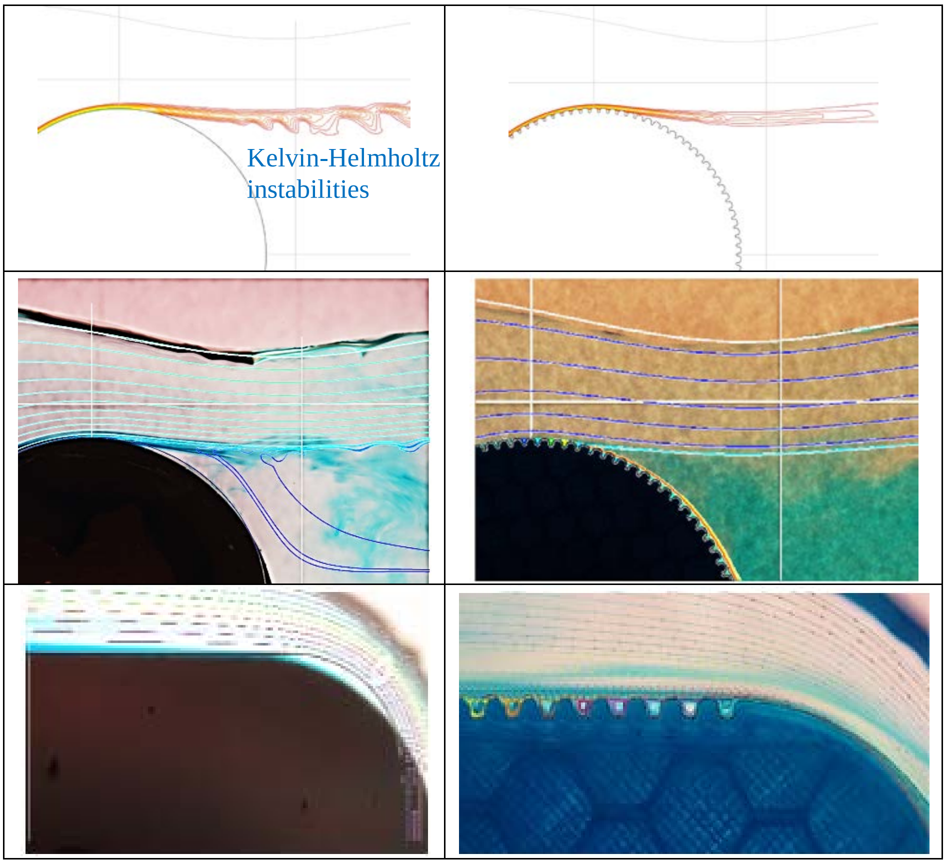

Fig. 8 – Comparison between smooth and grooved bodies: experimental and computed flow spectrum.

At the end, the numerical solutions are used to obtain value information about the flow in the vicinity of the bodies, including the influence of the wall micro-geometry on the location of the boundary layer detachment and the downstream wake formation, Fig. 9.

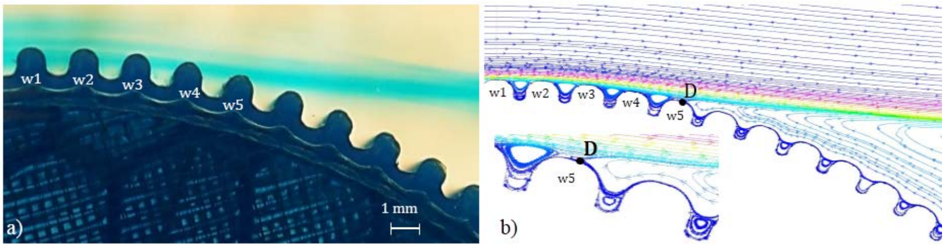

Fig. 9 – The visualisation (a) and computations (b) of the boundary layer detachment from the patterned immersed cylinder.

4. Conclusions

1. The results of the study are very promising and open the possibility to investigate in more details the influences of various forms of micro - geometries on the drag force of the immersed bodies.

2. The control of boundary layer by patterned surface is an old direction of study in fluid mechanics, but the applications of the topic in the free surface hydrodynamics are very actual.

3. Further numerical and experimental studies will be focused on two main directions: (*i*) optimize the numerical flow computation in the neighborhood of the patterned walls, (*ii*) perform experiments on immersed bodies with different micro-geometries.

Acknowledgements. This work was supported by grant of the Romanian National Authority for Scientific Research, CNDI-UEFISCDI, project number PN-II-PT-PCCA-2011-3.1-0052 and grant of the Ministry of National Education, CNCS – UEFISCDI, project number PN-II-ID-PCE-2012-4-0245. Nicoleta Octavia Tanase's work has been funded by the Sectoral Operational Programme Human Resources Development 2007-2013 of the Ministry of European Funds through the Financial Agreement POSDRU/159/1.5/S/132395.

REFERENCES

Broboană D., Muntean T., Bălan C., *Experimental and Numerical Studies of Weakly Elastic Viscous Fluids in a Hele - Shaw Geometry*, Proc. of the Romanian Academy, Series A, **8**, 219-233 (2007).

Chamorro L.P., Hill C., Morton S., Arndt R.E.A., Ellis C., Sotiropoulos F., *On the Interaction Between a Turbulent Open Channel Flow and an Axial-Flow Turbine*, J. Fluid Mech., **716**, 658-670 (2013).

El-Makdah A.M., Oweis G.F., *The Flow Past a Cactus-Inspired Grooved Cylinder*, Exp. Fluids, **54,** 1-16 (2013).

Launder B.E., Spalding D.B., *Mathematical Models of Turbulence*, Academic Press, London, 1972.

Lee S.J., Daichin, *Flow Past a Circular Cylinder Over a Free Surface: Interaction Between the Near Wake and the Free Surface Deformation*, J. Fluids and Struct., **19**, 1049-1059 (2004).

Rahimzadeh H., Maghsoodi R., Sarkardeh H., Tavakkol S., *Simulating Flow Over Circular Spillways by Using Different Turbulence Models*, Eng. Applic. of Computational Fluid Mech., **6**, 100-109, 2012.

Sheridan J., Lin J., Rockwell D., *Metastable States of a Cylinder Wake Adjacent to a Free Surface*, Phys Fluids, **7**, *9*, 2099-2101, 1995.

Tănase N.O., *Hydrodynamics of Free Surface Flow in Vicinity of Immersed Bodies in Transitory Subcritical Flow Regim* (*in Romanian*), Ph.D. Thesis, Power Engineering Faculty, "Politehnica" University of Bucharest, Romania, 2013.

Tănase N.O., Broboană D., Bălan C., *Flow Around an Immersed Cylinder in the Presence of free Surface*, Scientific Bulletin, UPB, **76**, Series D, 2, 259-266 (2014a).

Tănase N.O., Broboană D., Bălan C., *Free Surface Flow in Vicinity of an Immersed Cylinder*, Proc. of the Romanian Acad., Series A, **15**, 371-378 (2014b).

Tănase N.O., Broboană D., Bălan C., *Free Surface Flow Over the Broad - Crested Weir*, in IEEE Conference, 548-551, 2015.

*** Fluent Inc., Fluent 6.3 User's Manual, 2008.

INFLUENȚA SUPRAFEȚELOR STRUCTURATE ASUPRA SPECTRULUI CURGERII DIN VECINĂTATEA CORPURILOR IMERSATE

(Rezumat)

Lucrarea prezintă studiul experimental și numeric al curgerii cu suprafață liberă în jurul corpurilor imersate (cilindru și deversor cu prag lat). Scopul principal al lucrării este studiul influenței microgeometriei suprafeței corpurilor imersate, în funcție de adâncimea la care sunt imersate acestea pentru curgerea tranzitorie – turbulentă ($Re < 10^4$) în regim subcritic ($Fr < 1$) asupra spectrului curgerii și poziției punctului de desprindere a stratului limită.

BULETINUL INSTITUTULUI POLITEHNIC DIN IAŞI
Publicat de
Universitatea Tehnică „Gheorghe Asachi” din Iaşi
Volumul 62 (66), Numărul 2, 2016
Secţia
CONSTRUCŢII DE MAŞINI

CONSIDERATIONS ABOUT MATHEMATICAL MODELLING OF ELECTROCHEMICAL GRINDING PROCESSES

BY

CĂTĂLIN UNGUREANU[1,*] and RADU IBĂNESCU[2]

"Gheorghe Asachi" Technical University of Iaşi,
[1]Department of Machine Tools
[2]Department of Theoretical Mechanics

Received: July 26, 2016
Accepted for publication: November 29, 2016

Abstract. Electrochemical machining belongs to unconventional technologies category. This method is used for machining hard and extremely hard materials, employed, for example, in construction of tools for cutting and deformation. The machining process by electrochemical erosion is characterized by a very great number of working parameters, by electrical, mechanical or chemical nature. The mathematical modelling of the relationship between the machining parameters is a difficult problem. This paper presents experimental researches results accomplished by the authors for determining the dependence equations of some parameters that characterized the electrochemical grinding machining.

Keywords: unconventional technologies; electrochemical machining; mathematical modelling.

[*]Corresponding author; *e-mail*: cungurea@yahoo.com

1. Introduction

The process of electrochemical erosion-abrasive machining is based on the simultaneous pursuit of electrochemical dissolution processes combined with abrasive processes and electro discharge phenomena. In other words, the process occurs under the simultaneous action of the continuous electrical current, which leads to electrochemical decomposition of the metal under the action of the abrasive grains and which let off both the anodic dissolution products thus creating a mechanical deactivation and soluble components. Electro discharge phenomena, which generally have a negative impact on process performance, however contributes to improved productivity by pulling particulate matter by lightning. The literature indicates different values for the share of the two main factors (electrochemical and abrasive) in overall productivity by 98% material removed electrochemical and 2% removed about abrasive to equal shares of 50% for each factor (Kozak *et al*., 2001). This can be explained by the share of different electrical parameters and mechanical processing technology in the process.

2. The Structure of Electrochemical Abrasive Machining System

According to the general theory of systems, electrochemical erosion-abrasive is a system in which the input quantities are represented by all the conditions of work, and the outputs are represented, in the most general case, by the criteria for performance process evaluation. Detailed analysis of electrochemical grinding allowed separating and highlighting working conditions and criteria for performance process evaluation.

Electrochemical erosion-abrasive is characterized by a large number of operating parameters, which are system input quantities and describes and dictates the machining performances (Mc Geough, 1988). Compared to conventional grinding processes, this machining method involved besides electrical and chemical parameters. Working parameters representing system input quantities are represented by:

• electric regime: voltage, current, current density, flare mode;

• mechanical regime: abrasive wheel speed, longitudinal feed rate, oscillation stroke length, transverse advance;

• force: contact pressure, working electrodes gap width;

• abrasive disc electrode: the abrasive nature, grain size, concentration, nature of binder;

• electrolyte solution: chemical composition, concentration, specific gravity, specific heat, electrical conductivity, temperature, flow rate;

• the workpiece: composition, structure, physical and mechanical properties;

• machine-tool;

• fixtures.

Literature (Qu *et al*., 2015) presents a great number of criteria for evaluating performance for electrochemical abrasive machining processes. Process analysis concluded that the criteria for evaluation process performance can be:

• the total amount of material removed;
• total working time;
• amount of abrasive used;
• temperature of the electrolyte solution;
• forces developed in processing;
• power consumption to drive the grinding wheel;
• the power consumed by the electrochemical process;
• surface roughness processed;
• maximum form deviation;
• the total power consumed;
• cost spent for grinding wheel wearing;
• the total cost of processing.

3. Experimentals

For determining the depending equations of the criteria for assessing the performance of the electrochemical grinding process to the working parameters, the authors conducted an experimental program in the Department of Machine Tools and Tools to “Gheorghe Asachi” Technical University of Iaşi.

The research focused on determining the influence of voltage on productivity (Q) and the machining surface roughness (Ra), two of the most important criteria for process system evaluation.

The working parameters were: 0-14 V supply voltage, direct current, alternating double recovery, average processing speed 26 m/sec, contact pressure between abrasive disc electrode – workpiece 5 daN/cm^2, longitudinal advance 12 cd/min, height of the contact surface abrasive disc electrode - workpiece 6 mm.

The experimental results are shown in the diagrams of Figs. 1 and 2.

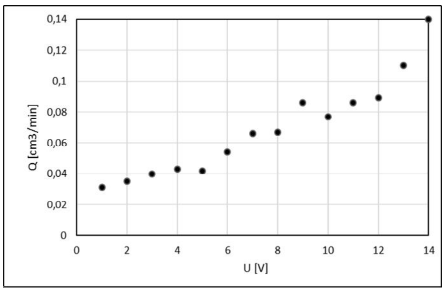

Fig. 1 – Voltage influence on productivity.

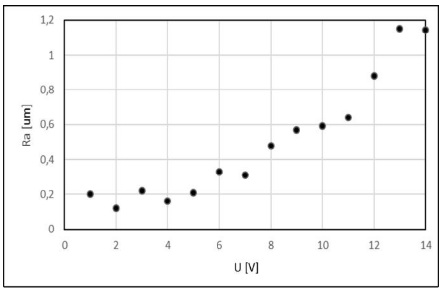

Fig. 2 – Voltage influence on surface roughness.

As shown in Fig. 1, increasing the voltage has a favorable effect on process productivity. But Fig. 2 shows that the same voltage increasing has an unfavorable effect on surface roughness.

These phenomenon, confirmed by the literature (Kozak, 2014), can be explained by the fact that voltage increase leads to enhanced electrochemical anodic dissolution, with positive influence on process productivity. At the same time, electric factor increasing leading out the development electro discharge phenomena, electric sparks appearance induces adverse effects on surface roughness.

4. Regression Functions Determination

Regression function means a mathematical expression, derived from processing experimental data, which approximates (estimated) dependencies between two or more variables of a system or process. Determining a regression function is required when the dependencies of those variables cannot be determined precisely enough about theoretical (Todincă and Geantă, 1999).

The method often used in such situations is to achieve an initial exploratory study, measuring the dependent variables for different values of process variables.

If we consider that the exact relationship (theoretical) dependency of a variable depending on other n variables in the process could be represented graphically by a surface in a space with n + 1 dimensions, the values derived experimentally can be represented by points in the space near this area. The points will not belong experimental area due to imprecision theoretical knowledge of process variables (*e.g.* due to measurement errors).

Thus, in situations where the relationship depends on one variable studied process and is expected to form the regression function to be determined fall within one category, it can use the method of least squares. If the relationship is dependent on many variables, it can get a polynomial regression function form using the response surfaces. In the cases where the two previous methods cannot be used, one of the methods derived from the iterative algorithms to solve the differential equation system can be applied.

Some of the above methods are sufficiently evolved so as not to be limited to determining expression of the regression function but also allows drawing conclusions concerning the correctness with which they were selected process variables and adequacy of accuracy with which they were performed measurements during experimental tests.

Thus, as an indicator of the adequacy of the model can be used model R^2 accuracy indicator expressed by the Eq. (1) (Todincă and Geantă, 1999):

$$R^2 = \frac{\sum_{i=1}^{n}\left(y_{icalc} - \overline{y}\right)^2}{\sum_{i=1}^{n}\left(y_{i\exp} - \overline{y}\right)^2} \tag{1}$$

In Eq. (1) y_{icalc} represents the values calculated using regression function, y_{iexp} - experimental values - average values of the objective function.

For experimental values shown in Figs. 1 and 2, several types of regression functions, shown in Figs. 3-10 were determined by using the Excel program.

A exponential regression type for the objective function Q is presented in Fig. 3. The determined relationship is shown in Eq. (2), the accuracy of the model and the indicator has the value (3).

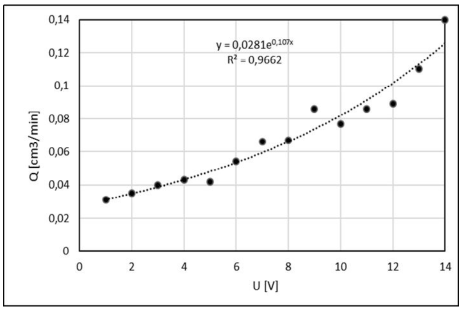

Fig. 3 – Exponential regression function.

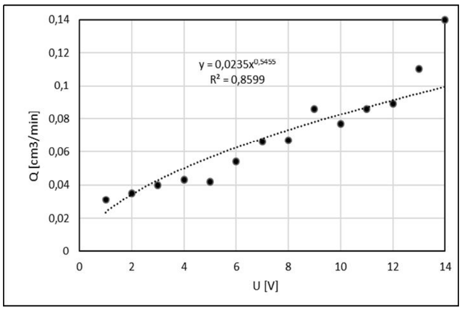

Fig. 4 – Power regression function.

$$y = 0.0281e^{0.107x} \tag{2}$$

$$R^2 = 0.9662 \tag{3}$$

A power type regression function for the objective function Q is presented in Fig. 4. The determined relationship is shown in Eq. (4), and the R^2 indicator has the value (5).

$$y = 0.0235x^{0.5455} \tag{4}$$

$$R^2 = 0.8599 \tag{5}$$

A linear regression function is presented in Fig. 5, and a polynomial one in Fig. 6. The determined relationships are shown in Eq. (6) and (8), and the R^2 indicator has the values (7) and (9).

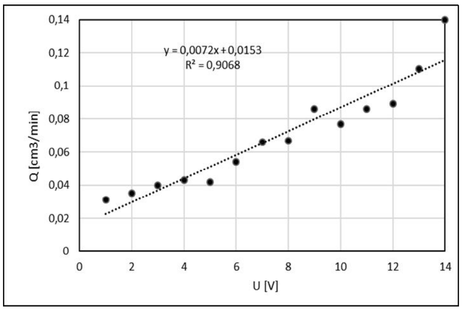

Fig. 5 – Linear regression function.

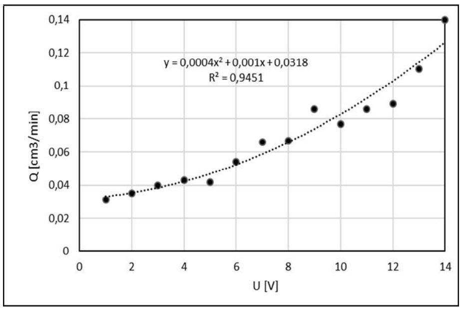

Fig. 6 – Polynomial regression function.

$$y = 0.0072x+0.015 \tag{6}$$

$$R^2 = 0.9068 \tag{7}$$

$$y = 0.000x^2 +0.001x+0.0318 \tag{8}$$

$$R^2 = 0.9451 \tag{9}$$

A exponential regression type for the objective function Ra is presented in Fig. 7. The determined relationship is shown in Eq. (10) and the model's accuracy indicator has the value (11).

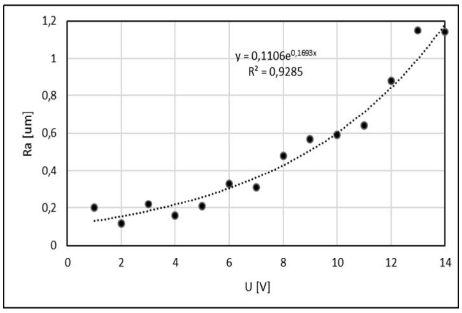

Fig. 7 – Exponential regression function.

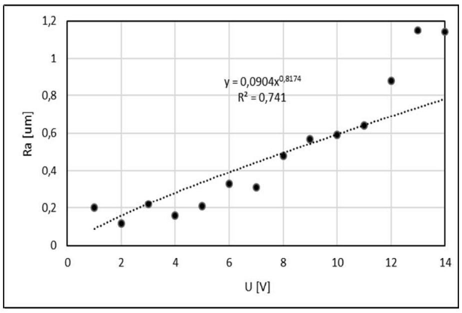

Fig. 8 – Power regression function.

$$y = 0.1106\mathrm{e}^{0.1693x} \tag{10}$$

$$R^2 = 0.9285 \tag{11}$$

A power type regression function for the objective function Ra is presented in Fig. 8. The determined relationship is shown in Eq. (12), and the R^2 indicator has the value (13).

$$y = 0.0904x^{0.8174} \tag{12}$$

$$R^2 = 0.741 \tag{13}$$

A linear regression function for Ra criteria is presented in Fig. 9, and a polynomial one in Fig. 10. The determined relationships are shown in Eq. (14) and (16), and the R^2 indicator has the values (15) and (17).

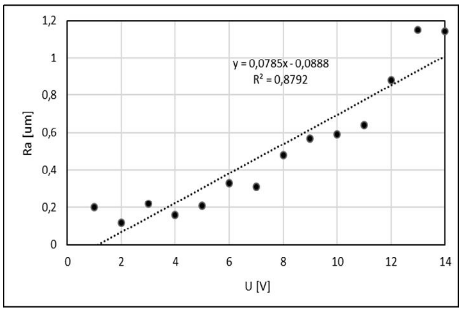

Fig. 9 – Linear regression function.

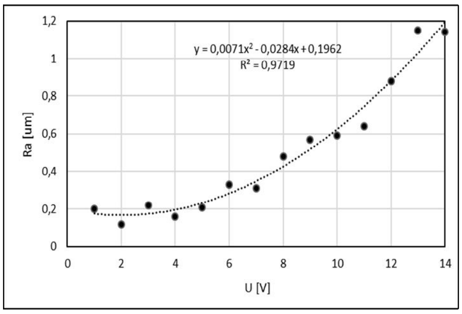

Fig. 10 – Polynomial regression function.

$$y = 0.0785x–0.0888 \tag{14}$$

$$R^2 = 0.8792 \tag{15}$$

$$y = 0.0071x^2–0.0284x+0.1962 \tag{16}$$

$$R^2 = 0.9719 \tag{17}$$

5. Conclusions

Based on calculate adequacy coefficients is possible to determine the precise regression function for the studied criteria.

Thus, the most precise regression function for Q objective is exponential function (R^2 = 0.9662) and for objective Ra polynomial function (R^2 = 0.9719).

Because in Ra case the regression function is a second degree polynomial, it is interesting to find out if a polynomial of degree higher than two provide a more accurate model. So, Eq. (18) show a third degree polynomial function for Ra criteria and (20) a four-degree polynomial function. The R^2 coefficients are shown in (19) and (21).

$$y = –0.00001x^3+0.0074x^2–0.0299x+0.1985 \tag{18}$$

$$R^2 = 0.9719 \tag{19}$$

$$y = 0.00003x^4 - 0.001x^3 + 0.0167x^2 - 0.0635x + 0.2314 \tag{20}$$

$$R^2 = 0.9721 \tag{21}$$

As can be seen, the coefficient R^2 does not have a significant increase so that it is considered as a second degree polynomial function provide a sufficiently accurate mathematical model.

REFERENCES

Kozak J., Oczos K., *Selected Problems of Abrasive Hybrid Machining*, J. of Materials Processing Technology, Vol. 109, No. 3, pp. 360-366 (2001).

Kozak J., *Analysis of Abrasive Electrochemical Grinding Process* (*AECG*), Proceedings of the World Congress on Engineering, 2014, Vol. II, July 2-4, London, U.K.

Mc Geough J.A., *Advanced Methods of Machining*, 1st Ed. Chapman and Hall, USA, 1988.

Qu N.S., Zhang Q.L., Fang X.L., Ye E.K., Zhu D., *Experimental Investigation on Electrochemical Grinding of Inconel 718*, 15th Machining Innovations Conference for Aerospace Industry, Procedia CIRP 35 (2015) pp. 16-19.

Todincă T., Geantă M., *Modelarea şi simularea proceselor chimice*, Ed. Politehnica, Timişoara, 1999.

CONSIDERAŢII PRIVIND MODELAREA MATEMATICĂ A PROCESELOR DE PRELUCRARE ELECTROCHIMICĂ ABRAZIVĂ

(Rezumat)

Procedeul de prelucrare prin eroziune electrochimică-abrazivă se bazează pe desfăşurarea simultană a unor procese de dizolvare electrochimică combinate cu procese de abrazare şi cu fenomene electroerozive. În vederea determinării ecuaţiilor de dependenţă ale criteriilor de evaluare a performanţelor procesului de prelucrare faţă de parametrii de lucru, autorii au efectuat un program experimental. Astfel s-a urmărit influenţa tensiunii de alimentare asupra productivităţii prelucrării şi asupra calităţii suprafeţelor prelucrate. Datele astfel obţinute au fost prelucrate cu ajutorul programului Excel şi s-au gasit mai multe tipuri de funcţii de regresie. Cu ajutorul criteriului R^2 s-a determinat cel mai adecvat model matematic.

BULETINUL INSTITUTULUI POLITEHNIC DIN IAŞI
Publicat de
Universitatea Tehnică „Gheorghe Asachi” din Iaşi
Volumul 62 (66), Numărul 2, 2016
Secţia
CONSTRUCŢII DE MAŞINI

HIGH-SPEED MACHINING IN DRY CUTTING CONDITIONS – AN OPPORTUNITY FOR CLEAN PRODUCTION – BRIEF REVIEW

BY

ANA MARIA BOCĂNEŢ[*] and IRINA COZMÎNCĂ

“Gheorghe Asachi” Technical University of Iaşi,
Faculty of Machines Manufacturing and Industrial Management

Received: November 15, 2016
Accepted for publication: December 16, 2016

Abstract. This paper presents a brief review on the latest researches in dry high-speed machining consisting in studies regarding the materials of the parts being cut, tools, methods and techniques used in order to investigate all the phenomena occurring during this type of processing. The results have shown that this field of research is continuously developing, emphasizing the possibilities of reaching an environmental-friendly manufacturing.

Keywords: Clean machining; dry cutting; high-speed cutting; cutting forces; tool’s wear.

1. Introduction

Metalworking industry is one of the leading industries in the world as it plays an essential role in the entire economy, which it supports through its products - machinery, industrial and technical equipment, machine tools, cutting tools, part’s material - boosting the development of other industries and economic sectors. It has the highest value in the total of industrial production

[*]Corresponding author; *e-mail*: anamaria_matei@hotmail.com

(35-45% in developed countries) and covers worldwide, over 30% of the workforce employed in industry.

Nowadays, the requirement for an environmental-friendly manufacturing is increasing around the world and also the demands for improved metals/materials. This creates new challenges for machining operations and place high demands for high performance cutting tools. Either is called environmental-friendly (Bhokse *et al*., 2015), green (Helu *et al*., 2012) or clean production (Krolczyk *et al*., 2016; Wang *et al*., 2014), it refers to a sustainable production, representing no threat to future generations and not being at the expense of future generations. Clean production does not have to mean increased financial investments. The goal is to reduce the environmental pollution in the process of manufacturing involving reduction of pollution generated by cooling/lubricating with coolants and emulsions (Krolczyk *et al*., 2016).

In his article (Landgraf, 2004), Greg Landgraf is presenting some of the advantages of dry cutting, as follows: the absence of water and atmosphere pollution; the resulted solid waste in form of debris can be recycled easier, without additional costs for cleaning the metalworking fluid, and also it can be sold with higher price; there is no danger for operator's health; dry cutting is economical considering that the costs attributed to the use of coolant are estimated to 16% of machining total cost ((Sharma *et al*., 2016) estimated this cost to 16 - 20%)), which is about 3-4 times the cutting tools cost; for high speed machining the using of dry cutting requires less cutting force; in interrupted cutting, such as milling, dry machining is suitable as it could improve the tool's life.

On the other hand, Neil Canter is presenting in his article (Canter, 2009), some of the advantages of dry cutting, similar to those presented above, but also some limitations of this type of machining, as follows: some companies have shown that the costs of maintaining and disposing the metalworking fluids are a lot less than 16% of company's total manufacturing costs; without using coolant, surface finish and tool life are severely affected as a tremendous amount of heat and friction is generated during the cutting process and this fact could significantly increase manufacturing costs and reduce productivity; not all machining operations are suitable for dry cutting; some alloys of metal being cut are more amenable to dry machining than others.

Other references (Graham *et al*., 2003; www.cnccookbook.com; www.theengineer.co.uk) highlight the advantages of dry cutting in high speed machining conditions and show the overcome of dry cutting limitations as the research in this field is evolving. Thus, in general, the increasing demand for hard machining and high-speed machining especially under dry cutting conditions has made many researchers to work in this field of development of manufacturing processes in order to obtain good surface finish and part accuracy, low energy consumption and maintaining long tool-life while reducing the impact of industrial activity on environment and health. These researches consist of analytical and experimental studies of cutting forces, chips formation, thermo elastic workpiece deformation, tool wear evolution, cutting temperature, cutting parameters optimization, surface roughness, cutting energy etc. when improved or hardened metals/materials are being cut in dry high-speed conditions (Wang *et al*., 2016; Zhang *et al.*, 2016; de Agustina *et al*., 2013; Salguero *et al*., 2013; Liu *et al*., 2009; Wang and Liu, 2015; Fang and Wu, 2009; Ma *et al*., 2015; Soler *et al*., 2015; Singh *et al*., 2015; Xie *et al*., 2013; van Hoof, 2014; Wang *et al*., 2014; Shashidhara and Jayaram, 2010), etc.

2. Workpiece Materials, Cutting Tools, Methods and Technologies for Studying Phenomena in Dry High-Speed Machining

Various studies regarding high-speed machining (HSM) in dry cutting conditions of the improved or hardened metals/materials were developed (Wang *et al*., 2016; Sugihara *et al*., 2015; de Agustina *et al*., 2013; Hanief *et al*., 2016; Salguero *et al*., 2013; Wang and Liu, 2015; Krishnakumar *et al*., 2015; Fang and Wu, 2009; Calatoru *et al*., 2008), etc. Some of these materials are suitable to this type of machining, some of them are submitted to research for optimizing the cutting process. Dry cutting has long been used with materials such as magnesium, which reacts with water, so common coolants are incompatible with it; most alloys of cast iron; carbon and alloyed steel that are relatively easy to machine and conduct heat well, allowing the chips to carry away most of the heat generated; some aluminum alloys.

However, the fast development of automotive, aerospace, shipbuilding, chemical or surgical industries requires improved and hardened metals/materials. Some of the HSM under dry conditions researches refer to these **materials**, as follows: Aluminium alloys (7050-T7451 (Wang *et al*., 2016; Wang *et al*., 2015), UNS A97075 (de Agustina *et al*., 2013), UNS A92024-T3 (Al-Cu) (Salguero *et al*., 2013), Al6061-T6 and Al7075-T6 (Zaghbani and Songmene, 2009), AlMgSi (Al 6061 T6) (Kalyan and Samuel, 2015), Al2016-T6 (Mithilesh Kumar Dikshit *et al*., 2014)), Titanium alloys (Ti–6Al–4V). (Fang and Wu, 2009), TC21 (Wu and To, 2015; Xie *et al*., 2013), Magnesium–calcium (MgCa) alloys (Salahshoor and Guo, 2011), hardened steels (Qing *et al*., 2010; Pawade *et al*., 2007), stainless steel (Krolczyk *et al*., 2016), gray cast iron (Tu *et al.*, 2016), superalloys (nickel-based Inconel 718), (Li *et al*., 2006) and Carbon Fiber Reinforced Polymers (Slamani *et al*., 2015; Uhlmann *et al*., 2016).

Also the open literature (Sugihara *et al*., 2015; Fang and Wu, 2009; Ma *et al*., 2015; Xie *et al*., 2013; Kalyan and Samuel, 2015; Martinho *et al*., 2008; Qing *et al*., 2010; Tu *et al.*, 2016; Kagnaya *et al*., 2014; Xing *et al*., 2014; Tian *et al*., 2013) covers an entire range of **cutting tools** used in HSM in dry conditions, such as high-performance carbide - multi-layer TiAlN coating, multi-layer hard coating consisting of distinct, alternating ultra-thin layers of

TiN (titanium nitride), TiAlN (titanium aluminum nitride), TiCN (titanium carbonitride) and lubrication coat -, PCBN, ceramics, diamond tools, PVD - applied nanolaminated TiSiN-TiAlN coated carbide tool.

Furthermore, in order to optimize the cutting conditions in dry HSM, the latest literature in this field presents studies conducted in most of the **manufacturing processes**: turning (De Agustina *et al*., 2013; Hanief *et al*., 2016; Bhokse *et al*., 2015; Pawade *et al*., 2007; Xie *et al*., 2013; Krolczyk *et al*., 2016; Kalyan and Samuel, 2015; Tu *et al.*, 2016), milling (Salguero *et al*., 2013; Zaghbani and Songmene, 2009; Mithilesh Kumar Dikshit *et al*., 2014; Singh *et al*., 2015; Kious *et al*., 2010; Li *et al*., 2006; Marinescu and Axinte, 2008; Lu *et al*, 2014; Tian *et al*., 2013; Smith *et al*., 2013), drilling (Harris *et al*., 2003), and gear hobbing (Claudin and Rech, 2009). In this papers, the phenomena occurring during HSM are studied, analyzed and compared using advanced **methods and technologies**, such as the analysis of variance (ANOVA), (Wang *et al*., 2016; De Agustina *et al*., 2013; Slamani *et al*., 2015; Pawade *et al*., 2007), finite element method (FEM) (Zhang *et al*., 2016; Wang and Liu, 2015; Bhokse *et al*., 2015; Ma *et al*., 2015; Puls *et al*., 2016; Wu and To, 2015; Kalyan and Samuel, 2015), finite element analysis (FEA) (Salahshoor and Guo, 2011; Calatoru *et al*., 2008), artificial neural network ANN, (Hanief *et al*., 2016; Krishnakumar *et al*., 2015), Taguchi method (Hanief *et al*., 2016), regression analysis (Hanief *et al*., 2016; Salguero *et al*., 2013; Fang and Wu, 2009), MATLAB (Hanief *et al*., 2016; Fang and Wu, 2009; Mithilesh Kumar Dikshit *et al*., 2014; Pawade *et al*., 2007), SFTC DEFORM software (Puls *et al*., 2016), MountainsMap 7.0 software (Krolczyk *et al*., 2016), Lab-VIEW (Krolczyk *et al*., 2016), field-programmable gate array (FPGA) (Sevilla-Camacho *et al*., 2015), PC208AX Sony data recorder (Li *et al*., 2006), LEICA MZ12 microscopy system (Li *et al*., 2006), optical microscope OLYMPUS SZ61TR (Tu *et al.*, 2016), scanning electron microscope (SEM), (Sugihara *et al*., 2015; Calatoru *et al*., 2008; Singh *et al*., 2015; Xie *et al*., 2013; Krolczyk *et al*., 2016; Kalyan and Samuel, 2015; Martinho *et al*., 2008; Qing *et al*., 2010; Pawade *et al*., 2007; Tu *et al.*, 2016; Uhlmann *et al*., 2016; Uhlmann *et al*., 2016; Kagnaya *et al*., 2014), Infrared radiation (IR) technology (Soler *et al*., 2015), ThermaVision A20V, ThermaCAM Researcher (Qing *et al*., 2010), Infinite Focus Measurement Machine (IFM) (Krolczyk *et al*., 2016), portable surface roughness-measuring instrument Mahr Perthometer Model M2 (Pawade *et al*., 2007), Kistler dynamometers and CNC machinery. Some of the results are presented as follows.

3. Research Background of the Phenomena Occurring in Dry High-Speed Machining

In the latest years, several studies dedicated to dry HSM of improved and hardened materials have been performed as to understand the cutting conditions, such as, cutting forces and temperature, chips formation, tool wear and surface quality, in order to machining process take place within a clean environment, obtaining, at the same time, proper results for productivity, tools and energy consumption and accuracy of the parts.

3.1. Cutting Forces in Dry HSM

Knowing the values of forces as an output data of the cutting process can provide both information about the input variables and parameters of the process, such as, cutting speed, feed, depth of cut, tool material and geometry, and about the machining process evaluation, as force's influence is usually reflected in other output variables, such as, surface quality, temperature, tool life and tool wear. This is the reason why several researches in dry HSM field are related to cutting forces (de Agustina *et al*., 2013; Hanief *et al*., 2016; Salguero *et al*., 2013; Fang and Wu, 2009; Zaghbani and Songmene, 2009; Bhokse *et al*., 2015; Mithilesh Kumar Dikshit *et al*., 2014; Pawade *et al*., 2007; Xie *et al*., 2013; Li *et al*., 2006; Tian X. *et al*., 2013; Thakur *et al*., 2012).

Kalyan C. and Samuel G.L. developed a study (Kalyan and Samuel, 2015) regarding the cutting forces when turning an AlMgSi alloy. To investigate the effect of feed rate and cutting speed on tangential cutting forces, PCD insert without edge preparation was used to turn the work material of 80 mm diameter at three different cutting speeds (400, 500 and 600 m/min), feed rates of 0.007, 0.02, 0.03 and 0.05 mm/rev and a depth of cut of 0.5 mm, without coolant. Also a finite element model to predict the forces during turning was developed. The size effect caused by the combined effect of material strengthening due to increase in strain gradient at low feed rates and the cutting edge geometry was considered in the developed finite element model. Some of the experimental results have shown that the tangential cutting forces reduce with increase in cutting speeds; this could be attributed to the thermal softening of the work material; all the three components of forces increase with the increase in cutting edge chamfer; as the ratio of feed rate and edge chamfer width reduces.

In their paper (Fang and Wu, 2009), N. Fang and Q. Wu made a comparative experimental study of high speed machining of two major aerospace materials – titanium alloy Ti–6Al–4V and Inconel 718. Based on extensive experimental data generated from 40 orthogonal high speed tube-cutting tests that involved five levels of cutting speeds and four levels of feed rates for each work material, the similarities and differences in machining the two materials were summarized as follows: for both materials, as the cutting speed increases, the cutting force, the thrust force, and the result force all decrease; however, the force ratio increases; for both materials, as the feed rate increases, the cutting force, the thrust force, the result force, as well as the force ratio all increase; under the same cutting conditions, the cutting force and the thrust force in machining Inconel 718 are higher than those in machining Ti–6Al–4V; the variation of the thrust force with the feed rate is smaller in machining Ti–6Al–4V than that in machining Inconel 718, especially at the lower cutting speeds. The final analysis revealed that the cutting forces in machining Ti–6Al–4V and Inconel 718 are governed by the interactions among work materials, tool geometry, and the cutting conditions.

3.2. Cutting Temperature in Dry HSM

The open literature in this field relates the cutting temperature to forces, material of the workpiece and tool, geometry of the inserts and cutting parameters, as data input, having an highly impact on tool's life and surface quality, as data output in dry high-speed machining process (Salahshoor and Guo, 2011; Calatoru *et al*., 2008; Soler, *et al*., 2015; Xie *et al*., 2013; Zaghbani and Songmene, 2009; Puls *et al*., 2016; Wu and To, 2015; Qing *et al*., 2010; Kagnaya *et al.*, 2014; Xing *et al*., 2014).

M. Salahshoor and Y.B. Guo developed a study (Salahshoor and Guo, 2011) on cutting mechanics in high speed dry face milling of biomedical magnesium–calcium MgCa0.8 alloy using internal state variable plasticity model. The results have shown the importance of knowing the cutting temperature when magnesium alloys are being cut, as the chip ignition, one of the most hazardous aspects in machining these alloys, does not occur in high-speed dry cutting with sharp PCD tools.

T. Kagnaya *et al*. investigated the damages of WC–6Co uncoated carbide tools during dry turning of AISI 1045 medium carbon steel at high speeds considering more parameters of influence, among which, the temperature played an important role (Kagnaya *et al.*, 2014). In order to take into account the temperature in tool wear analysis, the cutting tool temperature was measured through two isolated K-type thermocouples (ϕ = 0.25 mm). The results have shown that the temperature increases with increasing cutting speed and the reached temperature (about 600°C) is enough high to influence cutting tool wear. The highest temperatures recorded by the thermocouple nearest to the rake face, for the cutting speeds 100 m/min and 400 m/min after about 30 s of machining time, reached respectively of 400°C and 820°C. These temperatures were considered high enough to modify the tool material behavior and the microstructure of WC–6Co.

Zhenhua Qing *et al*. developed a study (Qing *et al*., 2010) on the high-speed and dry cutting chips of hardened alloy-steel with PCBN tool and the results have shown that the infrared image of the trail indicated that the machining generated a lot of cutting heat and most of the heat was carried by chip flow. Along with the cutting speed increasing, the temperature in shear zone increased and then decreased. The cutter were more likely to abrasive at Vc = 500 m/min, Vc = 600 m/min cutting speeds. When cutting speed increased to high as Vc = 800 m/min, a lot of cutting heat was carried out by chip, and the temperature changed little. The cutting temperature was lower than it at Vc = 500 m/min,Vc = 600 m/min cutting speed. The cutting process progressed smoothly. The paper concluded that it is suitable for PCBN cutter machining on 42CrMo hardened steel at high speed without cutting fluid.

3.3. Chip's Morphology in Dry HSM

The cutting principle during machining process refers to chip formation mechanism, in which the workpiece material undergoes large plastic deformation and the removed material is get rid of. Usually, the morphology of chips formed in the cutting speed range of HSM is serrated for ductile materials. The onset of serrated chip relates with cutting force and cutting temperature, tool wear and tool failure, quality of surface finish and accuracy of machined part, etc. (Wang and Liu, 2015; Xie *et al*., 2013; Salahshoor and Guo, 2011; Bhokse *et al*., 2015; Wu and To, 2015; Qing *et al*., 2010).

In their paper, (Wang and Liu, 2015), Bing Wang and Zhanqiang Liu investigated the influence of material constitutive parameters on the serrated chip formation during dry high speed machining (HSM) of Ti6Al4V alloys with finite element simulations and cutting experiments. Both the simulation and experimental results have shown that the serrated degree of chips increases with the cutting speed increasing until the chip becomes fragmented (Fig. 1). The cutting speed break point of chip morphology from serrated to fragmented for Ti6Al4V is about 2,500 m/min. Moreover, the average cutting force decreases with the cutting speed increasing.

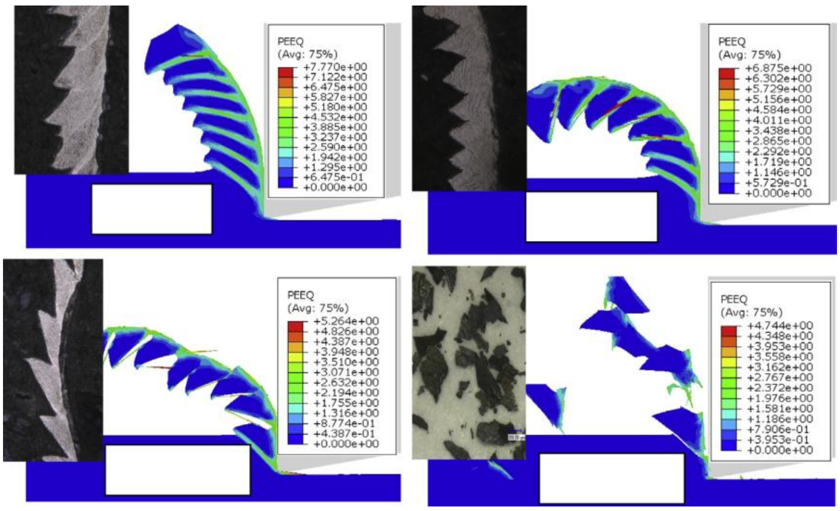

Fig. 1 − Variation of chip morphologies under different cutting speeds (Wang and Liu, 2015).

Hongbing Wu and Sandy To present in their paper, (Wu and To, 2015), an investigation on the cutting mechanism of a new high temperature and high strength titanium alloy named TC21 (Ti–6Al–2Sn–2Zr–3Mo–1Cr–2Nb) using the finite element method (FEM). A modified high temperature split Hopkinson pressure bar (SHPB) test system was employed to obtain the stress– strain curves of TC21 alloy under different temperatures and strain rates.

The study proved that the serrated chip occurred due to the thermal softening by the adiabatic effect. In addition, the results showed that the larger tool rake angle can decrease the extent of the serrated chip, and the cutting forces and the shear band frequency are sensitive to the tool rake angle during the machining process of TC21 alloy.

Zhenhua Qing *et al.* developed a study (Qing *et al*., 2010) on the high-speed hard and dry cutting chips of hardened alloy-steel with PCBN tool, showing that the chips are different from the cutting time. At the cutting beginning the chip is narrow, and saw-teeth-chip was at single side, whit low height and narrow width. The rough side squeezed severely and piles on each other. After a while of cutting, chip flows smoothly, become thinner, and saw-teeth-chip was seen at both sides. The saw tooth chip was different from one side to the other. The saw tooth could also been seen after tool wear down, and looked like band chip-low and small with the rough surface striation.

3.4. Tool’s Life and Tool Wear Monitoring in Dry HSM

Tool wear occurs under conditions of high temperatures (heat is generated and propagated), acting forces generate stresses and there is an internal friction in the deformed layers of material. This makes wear process of machining tools a very complex one, which results from interactions in the cutting zone. Selection of an appropriate cutting tool plays an important role in this perspective, whereas the selection of tool coating shall be adapted to appropriate types of machining. This is a significant factor, as coatings are applied in order to improve thermo physical, mechanical and tribological performance of machining process that depend also on machining process parameters (Krolczyk *et al*., 2016; Li *et al*., 2006; Martinho *et al*., 2008; Tu *et al.*, 2016; Claudin and Rech, 2009; Kagnaya*et al.*, 2014; Xing *et al*., 2014; Tian *et al*., 2013; Liu *et al*., 2013; Harris *et al*., 2003; Thakur *et al*., 2012).

In his paper, (Kious *et al*., 2010), Kious M. investigated the use of cutting force signal measurements to improve the on-line tool wear detection and the monitoring of coated tools in milling process by developing a predictive method of their wear. To achieve this goal, they have used the cutting force analysis to establish a relationship between the wear evolution and the cutting force variations. It was shown that the state of the tool wear observed by the microscope was related to results obtained by cutting force analysis. An automatic monitoring system of tool wear based on neural networks was implemented using the cutting condition, the insert type, the values of the variance, and the first harmonic of the cutting force as input vectors to estimate the tool wear.

Kagnaya T. investigated the damages of WC–6Co uncoated carbide tools during dry turning of AISI 1045 medium carbon steel at mean and high speeds, (Kagnaya *et al.*, 2014). The different wear micromechanisms were explained on the basis of different microstructural observations and analyses made by different techniques. The results have shown that the cutting tool wear depends on cutting speed. At conventional cutting speeds, a normal wear of the flank tool was observed. For high cutting speeds, a faster wear rate on the rake face was predominant. At a macroscopic scale, adhesion, abrasion and chipping wear were observed. The crater wear mode is dominant during machining AISI 1045 at high cutting speeds with WC–6Co cemented carbide cutting tools. The catastrophic wear mechanism of WC–6Co tools during high speed machining of AISI 1045 was activated by the coexistence of two main factors: severe tribological conditions on cutting tool and heat generation.

Krolczyk G.M. performed some researches regarding the tool life in dry turning of a duplex stainless steel using three different carbide tools, (Krolczyk *et al.*, 2016). The experiments were carried out in dry and cooling/lubricating conditions, and involved the measurements of surface roughness, cutting force components and tool life (Fig. 2).

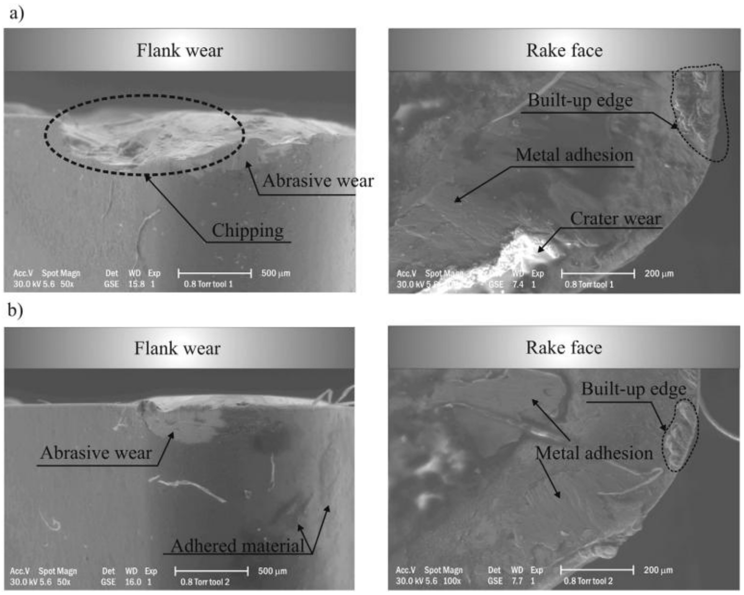

Fig. 2 − Topography of the tool point wear on cutting tools during DSS turning depending on the method of cooling: *a*) dry cutting;
b) lubricated cutting (Krolczyk *et al.*, 2016).

The results presented demonstrate that dry turning with the appropriately selected cutting tool grade and machining conditions induce almost three-fold growth of tool life in comparison to that obtained during cutting with fluids. The results have shown that the cutting tool life of duplex stainless steel depends on the following problems: difficult chip control and excessive thermal and mechanical loads of the cutting tool. It was also concluded that a rational solution in terms of energy consumption is machining without cooling, which involves combination of high cutting speed with low feed rate.

3.5. Surface Quality in Dry HSM

The general manufacturing problem can be described as the achievement of a predefined product quality with given equipment, cost and time constraints. Unfortunately, for some quality characteristics of a product such as surface roughness it is hard to ensure that these requirements will be met. In machining of parts, surface quality is one of the most specified customer requirements, reason why several researches in dry HSM field were dedicated to study this parameter (Kalyan and Samuel, 2015; Singh *et al*., 2015; Krolczyk *et al*., 2016; Uhlmann *et al*., 2016; Marinescu and Axinte, 2008; Pawade *et al*., 2007).

Pawade R.S. *et al*. studied the effect of cutting speed, feed rate, depth of cut and tool cutting edge geometry on cutting forces, surface roughness and surface damage in high-speed turning of Inconel 718 using PCBN tools, (Pawade *et al*., 2007). The experiments have shown that a 30° chamfer angle insert produce lower values of surface roughness at higher cutting speeds; SEM examination indicated that the presence of surface damage in the form of metal debris adhesion, smeared material, side flow and feed marks; the surfaces machined using 20° chamfered tool have fragments of carbide particles adhered on them; the machined surfaces at higher cutting speeds (*i.e*. 475 m/min) shown lesser flaws than those machined at 125 and 300 m/min cutting speeds.

Krolczyk G.M., in his study, (Krolczyk *et al*., 2016), also referred to the surface quality, showing that the roughness profile, after turning with a multi-layer coated tool with cooling led to many more tribological disturbances than in the case of machining without cooling – the surface roughness profile shape can prove a transverse plastic flow of the material in the cutting zone.

Kalyan C. and Samuel G.L. presented in their study (Kalyan and Samuel, 2015), also some results regarding the surface roughness, showing that best surface finish (Ra of 50 nm) was achieved at the lowest feed rate of 0.007 mm/rev at cutting speeds of 300, 400 and 600 m/min; the effect of feed rate is more pronounced on the surface finish than the cutting speed; the minimum feed rate for achieving the best surface finish in high speed turning (cutting speed of 1200 m/min) was found for each insert with different edge chamfer widths; the minimum feed rates obtained are 0.04 mm/rev for 20 μm edge chamfer width, 0.06 mm/rev for 40 μm edge chamfer width, 0.09 mm/rev for 60 μm edge chamfer width and 0.09 mm/rev for 80 μm edge chamfer width; the surface roughness is found to decrease with increase in nose radius when the feed rate is in the region of shearing dominated mode of cutting and the surface roughness is found to increase with increase in nose radius when the feed rate is in the region of ploughing dominated mode of cutting after a particular value of nose radius due to the domination of ploughing action at higher values of nose radius at low feed rate and depth of cut.

4. Conclusions

This paper presents some of the latest researches in the field of dry high-speed manufacturing, aiming to understand the possibilities of a clean production in all machining processes. The following conclusions could be drawn.

1. Researchers agree that HSM in dry conditions is a way to reach clean production, non-polluting and not involving extra costs.

2. Ductile materials (such as, medium and low carbon steels) of the workpiece easily allow this type of processing; however, there are recent studies showing the continuous research of dry HSM of low or medium carbon parts.

3. Problems occur in the case of very hard or improved materials increasingly used in the automotive and aerospace industry, materials that require special working conditions, reason why many studies in dry HSM are related to these materials.

4. High speed dry cutting can be performed in almost all processing methods, fewer studies being developed for drilling and grinding, whereas the removal of coolant from process is almost impossible; in these cases there are analyzed and developed alternative methods of cooling.

5. For certain types of materials it was proven that high-speed cutting is developing better in dry cutting conditions, especially in certain processes, such as milling.

6. Literature study shows the possibility to develop new researches in HSM under dry cutting conditions, both in case of conventional materials (low and medium carbon steels), and especially for hard materials (hardened steels, superalloys), given their continuous improvement.

REFERENCES

Bhokse V., Chinchanikar S., Anerao P., Kulkarni A., *Experimental Investigations on Chip Formation and Plowing Cutting Forces during Hard Turning*, Materials Today: Proceedings 2, online at www.sciencedirect.com, 3268-3276 (2015).

Calatoru V.D., Balazinski M., Mayer J.R.R., Paris H., L'Esperance G., *Diffusion Wear Mechanism during High-Speed Machining of 7475-T7351 Aluminum Alloy* *with Carbide End Mills*, Wear 265, online at www.elsevier.com/locate/wear, 1793-1800 (2008).

Canter N., *The Possibilities and Limitation of Dry Machining*, online at http://www.uscti.com/u_pages/publications/pdfs/ItemGDryMachiningMarch2009CanterSTLEStark.pdf (2009).

Claudin C., Rech J., *Development of a New Rapid Characterization Method of Hob's Wear Resistance in Gear Manufacturing - Application to the Evaluation of Various Cutting Edge Preparations in High Speed Dry Gear Hobbing*, Journal of Materials Processing Technology 209, online at doi:10.1016/j.jmatprotec.2009.02.014, 5152-5160 (2009).

de Agustina B., Bernal C., Camacho A.M., Rubio E.M., *Experimental Analysis of the Cutting Forces Obtained in Dry Turning Processes of UNS A97075 Aluminium Alloys*, Procedia Engineering 63, online at www.sciencedirect.com, 694-699 (2013).

Fang N., Wu Q., *A Comparative Study of the Cutting Forces in High Speed Machining of Ti–6Al–4V and Inconel 718 with a Round Cutting Edge Tool*, Journal of Materials Processing Technology 209, online at www.elsevier.com/locate/jmatprotec, 4385-4389 (2009).

Graham D., Huddle D., McNamara D., *Machining Dry Is Worth A Try*, online at www.mmsonline.com/articles/machining-dry-is-worth-a-try, (2003), accessed on 11th November 2016.

Hanief M., Wani M.F., Charoo M.S., *Modeling and Prediction of Cutting Forces during the Turning of Red Brass* (*C23000*) *Using ANN and Regression Analysis*, Eng. Sci. Tech., Int. J., online at http://dx.doi.org/10.1016/j.jestch.2016.10.019 (2016).

Harris S.G., Doyle E.D., Vlasveld A.C., Audy J., Quick D., *A Study of the Wear Mechanisms of Ti1−XAlXN and Ti1−X−YAlXCrYN Coated High-Speed Steel Twist Drills under Dry Machining Conditions*, Wear, Vol. **254**, *7-8*, online at http://dx.doi.org/10.1016/S0043-1648(03)00258-8, 723-734 (2003).

Helu M., Behmann B., Meier H., Dornfeld D. *et al*., *Impact of Green Machining Strategies on Achieved Surface Quality*, CIRP Annals - Manufacturing Technology 61:1, online at http://dx.doi.org/10.1016/j.cirp.2012.03.092, 55-58 (2012).

Kalyan C., Samuel G.L., *Cutting Mode Analysis in High Speed Finish Turning of AlMgSi Alloy using Edge Chamfered PCD Tools*, Journal of Materials Processing Technology 216, online at http://dx.doi.org/10.1016/j.jmatprotec.2014.09.003, 146-159 (2015).

Kagnaya T., Boher C., Lambert L., Lazard M., Cutard T., *Microstructural Analysis of Wear Micromechanisms of WC–6Co Cutting Tools during High Speed Dry Machining*, Int. Journal of Refractory Metals and Hard Materials 42, online at http://dx.doi.org/10.1016/j.ijrmhm.2013.08.017, 151-162 (2014).

Kious M., Ouahabi A., Boudraa M., Serra R., Cheknane A., *Detection Process Approach of Tool Wear in High Speed Milling*, Measurement 43, online at doi:10.1016/j.measurement.2010.08.014, 1439-1446 (2010).

Krishnakumar P., Rameshkumar K., Ramachandran K.I., *Tool Wear Condition Prediction Using Vibration Signals in High Speed Machining (HSM) of Titanium (Ti-6Al-4V) Alloy*, Procedia Computer Science 50, online at www.sciencedirect.com, 270-275 (2015).

Krolczyk G.M., Nieslony P., Maruda R.W., Wojciechowski S., *Dry Cutting Effect in Turning of a Duplex Stainless Steel as a Key Factor in Clean Production*, Journal of Cleaner Production, online at http://dx.doi.org/10.1016/j.jclepro.2016.10.136, 1-12 (2016).

Landgraf G., *Dry Goods - Factors to Consider when Dry or Near-Dry Machining*, Cutting tool Eng, **56**, *1*, 28-35 (2004).

Li H.Z., Zeng H., Chen X.Q., *An Experimental Study of Tool Wear and Cutting Force Variation in the End Milling of Inconel 718 with Coated Carbide Inserts*, Journal of Materials Processing Technology 180, online at doi:10.1016/j.jmatprotec.2006.07.009, 296-304 (2006).

Li A., Zhao J., Luo H. *et al*., *Progressive Tool Failure in High-Speed Dry Milling of Ti-6Al-4V Alloy with Coated Carbide Tools*, Int. J. Adv. Manuf. 58: 465, online at doi:10.1007/s00170-011-3408-1 (2012).

Liu Y.J., Huang J.B., Qing M.Y., Xia W., Tang Y., *High Speed Machining of AISI 52100 Steel*, Advanced Materials Research Online, ISSN: 1662-8985, Vol. **69-70**, online at doi:10.4028/www.scientific.net/AMR.69-70.466, 466-470 (2009).

Liu Z., An Q., Xu J., Chen M., Han S., *Wear Performance of (nc-AlTiN)/(a-Si3N4) Coating and (nc-AlCrN)/(a-Si3N4) Coating in High-Speed Machining of Titanium Alloys under Dry and Minimum Quantity Lubrication (MQL) Conditions*, Wear Vol. **305**, *1-2*, online at http://dx.doi.org/10.1016/j.wear.2013.02.001, 249-259 (2013).

Lu L. *et al*., *Microstructure and Cutting Performance of CrTiAlN Coating for High-Speed Dry Milling*, Trans. Nonferrous Met. Soc. China 24, online at DOI: 10.1016/S1003-6326(14)63256-8, 1800-1806 (2014).

Ma J., Duong N.H., Lei S., *Numerical Investigation of the Performance of Microbump Textured Cutting Tool in Dry Machining of AISI 1045 Steel*, Journal of Manufacturing Processes 19, online at http://dx.doi.org/10.1016/j.jmapro.2014.10.001, 194-204 (2015).

Martinho R.P., Silva F.J.G., Baptista A.P.M., *Cutting Forces and Wear Analysis of Si3N4 Diamond Coated Tools in High Speed Machining*, Vacuum 82, online at doi:10.1016/j.vacuum.2008.03.065, 1415-1420 (2008).

Marinescu I., Axinte D.A., *A Critical Analysis of Effectiveness of Acoustic Emission Signals to Detect Tool and Workpiece Malfunctions in Milling Operations*, International Journal of Machine Tools & Manufacture 48, online at doi:10.1016/j.ijmachtools.2008.01.011, 1148-1160 (2008).

Mithilesh Kumar Dikshit, Asit Baran Puri, Atanu Maity and Amit Jyoti Banerjee, *Analysis of Cutting Forces and Optimization of Cutting Parameters in High-Speed Ball-End Milling Using Response Surface Methodology and Genetic Algorithm*, Procedia Materials Science 5, online at www.sciencedirect.com, 1623-1632 (2014).

Pawade R.S., Suhas S. Joshi, Brahmankar P.K., Rahman M., *An Investigation of Cutting Forces and Surface Damage in High-Speed Turning of Inconel 718*, Journal of Materials Processing Technology 192–193, online at doi:10.1016/j.jmatprotec.2007.04.049, 139-146 (2007).

Puls H., Klocke F., Döbbeler B., Peng B., *Multiscale Modeling of Thermoelastic Workpiece Deformation in Dry Cutting*, Procedia CIRP 46, online at doi: 10.1016/j.procir.2016.03.195 , 27-30 (2016).

Qing Z., Zuo D., Xie F., Zhang C., *Trail Investigation on Chip of High-speed and Dry Cutting on Hardened Steel with PCBN Tool*, Advanced Materials Research Online: 2010-10-19, ISSN: 1662-8985, Vol. **142**, online at doi:10.4028/www.scientific.net/AMR.142.26, 26-30 (2010).

Salguero J., Batista M., Calamaz M., Girot F., Marcos M., *Cutting Forces Parametric Model for the Dry High Speed Contour Milling of Aerospace Aluminium Alloys*, Procedia Engineering 63, online at www.sciencedirect.com, 735-742 (2013).

Salahshoor M., Guo Y.B., *Cutting Mechanics in High Speed Dry Machining of Biomedical Magnesium–Calcium Alloy Using Internal State Variable Plasticity Model*, Int. J. of Machine Tools & Manuf. 51, online at www.elsevier.com/locate/ijmactool, 579-590 (2011).

Sevilla-Camacho P.Y., Robles-Ocampo J.B., Jauregui-Correa J.C., Jimenez-Villalobos D., *FPGA-Based Reconfigurable System for Tool Condition Monitoring in High-Speed Machining Process*, Measurement 64, online at http://dx.doi.org/10.1016/j.measurement.2014.12.037, 81-88 (2015).

Sharma A.K., Tiwari A.K., Dixit A.R., *Effects of Minimum Quantity Lubrication (MQL) in Machining Processes Using Conventional and Nanofluid Based Cutting Fluids: A Review*, J. Clean. Prod. 127, 1-18 (2016).

Shashidhara Y.M., Jayaram S.R., *Vegetable Oils as a Potential Cutting Fluid an Evolution*, Tribol. Int. 43, 1073-1081 (2010).

Singh K.K., Kartik V., Singh R., *Modeling Dynamic Stability in High-Speed Micro Milling of Ti–6Al–4V Via Velocity and Chip Load Dependent Cutting Coefficients*, International Journal of Machine Tools & Manufacture 96, online at http://dx.doi.org/10.1016/j.ijmachtools.2015.06.002 , 56-66 (2015).

Slamani M., Gauthier S., Chatelain J.-F., *A Study of the Combined Effects of Machining Parameters on Cutting Force Components during High Speed Robotic Trimming of CFRPs*, Measurement 59, online at http://dx.doi.org/10.1016/j.measurement.2014.09.052, 268-283 (2015).

Smith I.J., Münz W.D., Donohue L.A., Petrov I., Greene J.E., *Improved Ti1–xAlxN PVD Coatings for Dry High Speed Cutting Operations*, Surf. Eng. 14, 1998:1, online at http://dx.doi.org/10.1179/sur.1998.14.1.37, 37-42 (2013).

Soler D., Aristimuńo P., Garay A., Arrazola P. J., *Uncertainty of Temperature Measurements in Dry Orthogonal Cutting of Titanium Alloys*, Infrared Physics & Technology 71, online at http://dx.doi.org/10.1016/j.infrared.2015.04.001, 208-216 (2015).

Sugihara T., Nishimoto Y., Enomoto T., *On-Machine Tool Resharpening Process for Dry Machining of Aluminum Alloys Employing LME Phenomenon*, Precision Engineering 40, online at http://dx.doi.org/10.1016/j.precisioneng.2014.12.005, 241-248 (2015).

Tian X., Zhao J., Zhao J. et al., *Effect of Cutting Speed on Cutting Forces and Wear Mechanisms in High-Speed Face Milling of Inconel 718 with Sialon Ceramic Tools*, Int. J. Adv. Manuf. Technol. 69: 2669, online at doi:10.1007/s00170-013-5206-5214 (2013).

Thakur D.G., Ramamoorthy B., Vijayaraghavan L., *Some Investigations on High Speed Dry Machining of Aerospace Material Inconel 718 Using Multicoated Carbide Inserts*, Materials and Manufacturing Processes, Vol. **27**, *10*, online at http://dx.doi.org/10.1080/10426914.2011.654158 (2012).

Tu G., Wu S., Liu J., Long Y., Wang B., *Cutting Performance and Wear Mechanisms of Sialon Ceramic Cutting Tools at High Speed Dry Turning of Gray Cast Iron*, Int. Journal of Refractory Metals and Hard Materials 54, online at http://dx.doi.org/10.1016/j.ijrmhm.2015.08.007, 330-334 (2016).

Uhlmann E., Richarz S., Sammler F., Hufschmied R., *High Speed Cutting of Carbon Fibre Reinforced Plastics*, Procedia Manufacturing 6, online at doi: 10.1016/j.promfg.2016.11.015, 113-123 (2016).

van Hoof B., *Organizational Learning in Cleaner Production among Mexican Supply Networks*, J. Clean. Prod. 64, 115-124 (2014).

Wang B., Liu Z., Song Q., Wan Y., Shi Z., *Proper Selection of Cutting Parameters and Cutting Tool Angle to Lower the Specific Cutting Energy during High Speed Machining of 7050-T7451 Aluminum Alloy*, Journal of Cleaner Production 129, online at http://dx.doi.org/10.1016/j.jclepro.2016.04.071, 292-304 (2016).

Wang B., Liu Z., *Shear Localization Sensitivity Analysis for Johnson–Cook Constitutive Parameters on Serrated Chips in High Speed Machining of Ti6Al4V*, Simulation Modelling Practice and Theory 55, online at http://dx.doi.org/10.1016/j.simpat.2015.03.011, 63-76 (2015).

Wang W.-K., Lu W.-M., Wang S.-W., *The Impact of Environmental Expenditures on Performance in The U.S. Chemical Industry*, J. Clean. Prod. 64, 447-456 (2014).

Wang B., Liu Z., Su G., Song Q., Ai X., *Investigations of Critical Cutting Speed and Ductile-to-Brittle Transition Mechanism for Workpiece Material in Ultra-High Speed Machining*, International Journal of Mechanical Sciences 104, online at http://dx.doi.org/10.1016/j.ijmecsci.2015.10.004, 44-59 (2015).

Wu H., To S., *Serrated Chip Formation and Their Adiabatic Analysis by Using the Constitutive Model of Titanium Alloy in High Speed Cutting*, Journal of Alloys and Compounds 629, online at http://dx.doi.org/10.1016/j.jallcom.2014.12.230, 368-373 (2015).

Xie J., Luo M.J., Wu K.K., Yang L.F., Li D.H., *Experimental Study on Cutting Temperature and Cutting Force in Dry Turning of Titanium Alloy Using a Non-Coated Micro-Grooved Tool*, International Journal of Machine Tools & Manufacture 73, online at http://dx.doi.org/10.1016/j.ijmachtools.2013.05.006 , 25-36 (2013).

Xing Y., Deng J., Zhao J., Zhang G., Zhang K., *Cutting Performance and Wear Mechanism of Nanoscale and Microscale Textured Al2O3/TiC Ceramic Tools in Dry Cutting Of Hardened Steel*, Int. Journal of Refractory Metals and Hard Materials 43, online at http://dx.doi.org/10.1016/j.ijrmhm.2013.10.019, 46-58 (2014).

Yang H., Qing Z., Xie F., Zhang C., *Experiments on High-speed and Dry Cutting with PCBN Tool*, Key Engineering Materials Online: 2010-03-02, ISSN: 1662-9795, Vol. **431-432**, online at doi:10.4028/www.scientific.net/KEM.431-432.114, 114-117 (2010).

Zaghbani I., Songmene V., *A Force-Temperature Model Including a Constitutive Law for Dry High Speed Milling of Aluminium Alloys*, Journal of materials processing technology 209, online at www.elsevier.com/locate/jmatprotec, 2532-2544 (2009).

Zhang K., Liu Z., Wang Y., Liu Y., *Method of Strain-Rate Difference Calculation in High-Speed Metal Cutting*, Measurement 91, online at http://dx.doi.org/10.1016/j.measurement.2016.05.091, 474-478 (2016).

* * * *The Fascinating World of Dry and Near-Dry Machining*, online at www.cnccookbook.com/CCDryMachining.html, accessed on 14th November 2016.

* * * *The Benefits of Dry Machining*, online at www.theengineer.co.uk/the-benefits-of-dry-machining/, (2016), accessed on 14th November 2016.

PRELUCRAREA CU VITEZE RIDICATE ÎN CONDIȚII DE AȘCHIERE USCATĂ – O OPORTUNITATE A PRODUCȚIEI CURATE – SCURTĂ PREZENTARE

(Rezumat)

Lucrarea prezintă o scurtă descriere a ultimelor cercetări din domeniul prelucrării metalelor în condiții de așchiere uscată cu viteze ridicate, constând în studii cu privire la materialele pieselor prelucrate, scule așchietoare, metode și tehnici utilizate pentru investigarea fenomenelor care apar în timpul acestui tip de prelucrare. Rezultatele au arătat că acest domeniu de cercetare este în continuă dezvoltare, subliniind posibilitățile de a se ajunge la un tip de prelucrare prin așchiere prietenos cu mediul înconjurator.

BULETINUL INSTITUTULUI POLITEHNIC DIN IAŞI
Publicat de
Universitatea Tehnică „Gheorghe Asachi” din Iaşi
Volumul 62 (66), Numărul 2, 2016
Secţia
CONSTRUCŢII DE MAŞINI

CONTRASTIVE ANALISYS OF THE FLOW AROUND AN AIRFOIL

BY

EUGEN-VLAD NĂSTASE[*]

"Gheorghe Asachi" Technical University of Iaşi,
Department of Fluid Mechanics Fluid Machinery and Fluid Power Systems

Received: December 5, 2016
Accepted for publication: December 20, 2016

Abstract. The objective of the application is to determine, through Computational Fluid Dynimics (CFD) of Ansys, the pressure coefficient distribution around an airfoil placed in a fluid stream. If known distribution of pressure can then determine the aerodynamic force and its components: the drag force and the lift force. The velocity of the air stream is 50 m/s and air density is 1.16 kg/m^3 for an airfoil with chord c = 150 mm, span b = 110 mm and an angle of attack α = 18º. Finally, the results predicted by 2D simulation will be compared with experimental data measured in wind tunnel.

Keywords: airfoil; lift; drag; flow simulation; CFD.

1. Introduction

In the field of fluid dynamics, an area of significant practical importance is the study of airfoils. Generally, an airfoil is defined as the cross section of a body that is placed in an airstream in order to produce a useful aerodynamic force in the most efficient manner possible. This force is used for different purposes such as the cross sections of wings, propeller blades,

[*]Corresponding author; *e-mail*: nastase_eugenvlad@yahoo.com

windmill blades, compressor and turbine blades in a jet engine, and hydrofoils are examples of airfoils (Şahin and Acir, 2015).

2. General Considerations

The basic geometry of an airfoil is shown in Fig. 1. The leading edge is the point at the front of the airfoil that has maximum curvature. The trailing edge is defined similarly as the point of maximum curvature at the rear of the airfoil. The chord line is a straight line connecting the leading and trailing edges of the airfoil. The chord length, or simply chord is the length of the chord line and is the characteristic dimension of the airfoil section (Kevadiya, 2013). Aerodynamic forces result from the pressure distribution over the surface of airfoil.

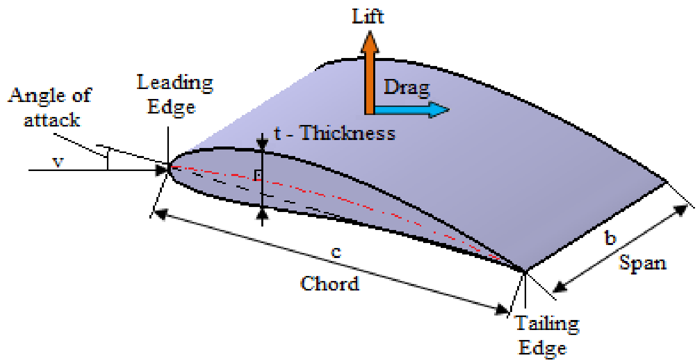

Fig. 1 – Geometry of an airfoil.

The drag on a body in an oncoming flow is defined as the force on the body in a direction parallel flow direction.

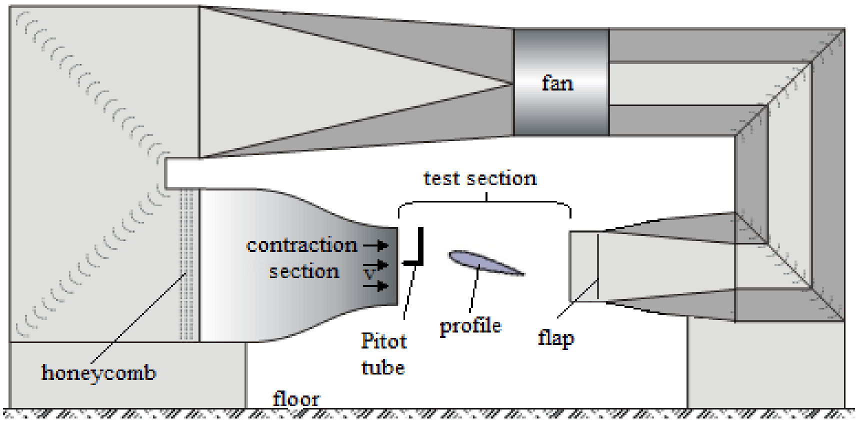

Fig. 2 – Layout of the profile in wind tunnel.

For experimental determinations the profile is installed in wind tunnel (Fig. 2). The pressure distribution around the airfoil is obtained from 18 pressure taps, connected using flexible tubes to the measuring instrument. Positioning of pressure taps and measured values are given in Table 1.

Table 1
Experimental Data

Tap number	1	2	3	4	5	6	7	8	9
Position [mm]	0	2	10	19	34	56	78	102	130
10^{-3}* Δp [N/m^2]	-0.34	1.31	1.13	0.55	0.47	0.41	0.29	0.37	0.04
Tap number	10	11	12	13	14	15	16	17	18
Position [mm]	150	124	102	75	56	33.5	19	9.5	1.5
10^{-3}*Δp [N/m^2]	0.22	-0.01	-0.15	-0.34	-0.73	-1.24	-1.66	-2.64	-3.97

To calculate the pressure coefficient (Sagat *et al*., 2012) is used Eq. (1):

$$K_p = \frac{2 \cdot \Delta p}{\rho \cdot v^2} \tag{1}$$

Using Eq. (2) and the data in Table 1 traces the pressure coefficient distribution around profile (Fig. 2). This is experimental data.

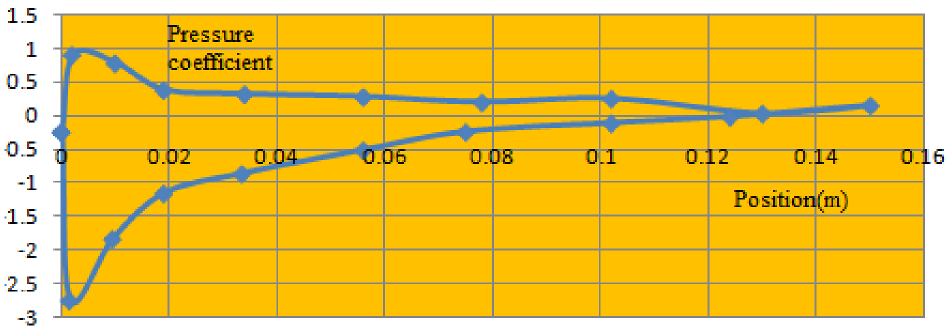

Fig. 2 – The pressure coefficient determined by experiment.

Lift and drag, depends upon the pressure distribution and velocity distribution of an airfoil (Kandwal and Singh, 2012) and can be determined using Eq. (2) and Eq. (3) (Şahin and Acir, 2015):

$$F_L = \frac{1}{2}\rho A v^2 C_L \tag{2}$$

$$F_D = \frac{1}{2}\rho A v^2 C_D \tag{3}$$

3. Results of Simulation

Ansys simulation results are presented below. In Fig. 3 you can see the distribution of velocity around the profile.

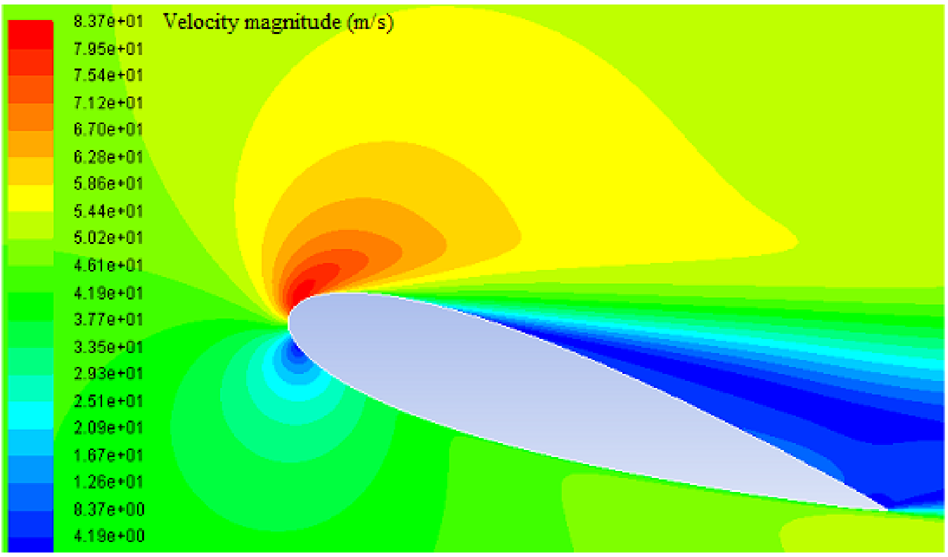

Fig. 3 – Contour of velocity magnitude.

In Fig. 4 is shown the total pressure, and in Fig. 5 is static pressure distribution.

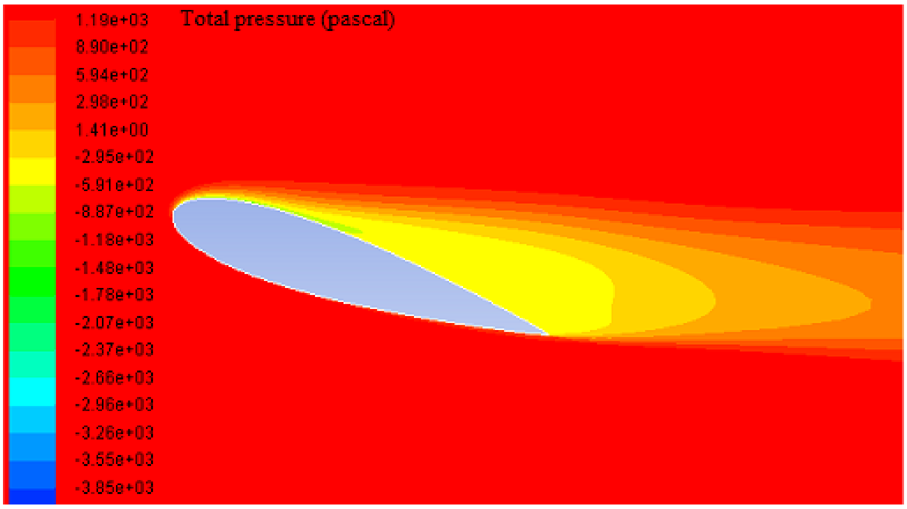

Fig. 4 – Total pressure around the airfoil.

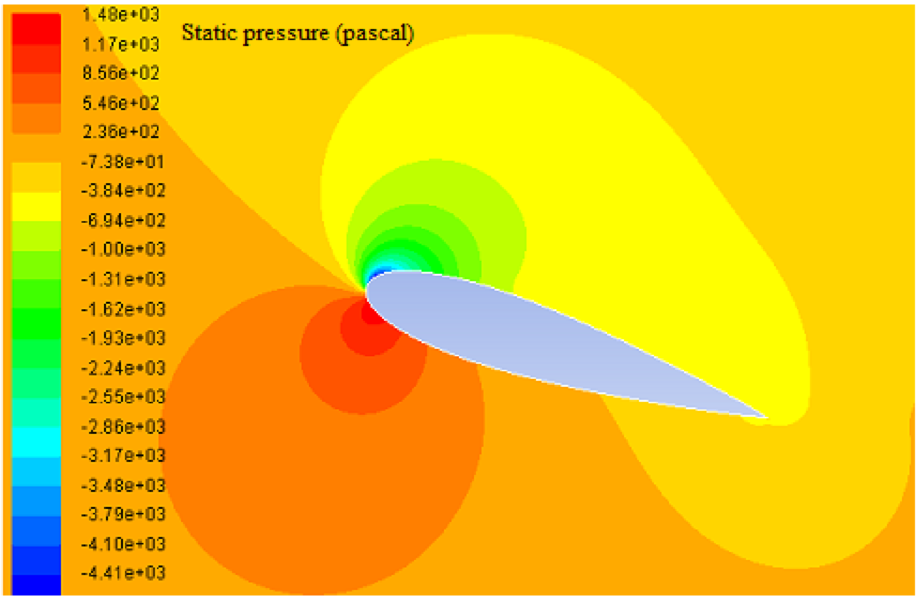

Fig. 5 – The static pressure contour.

In Fig. 6 you can see the distribution of pressure around the profile generated by simulation with Ansys and determined in the wind tunnel.

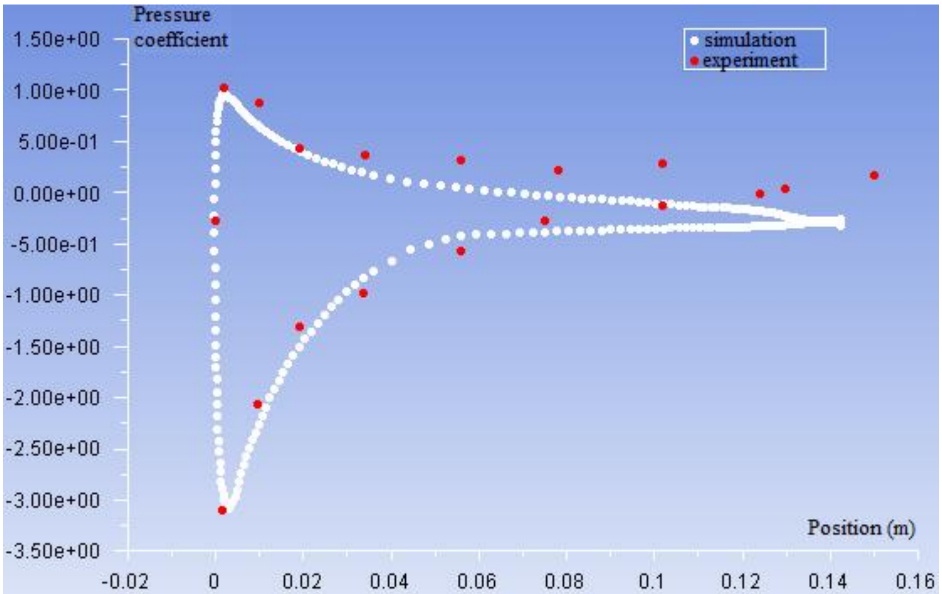

Fig. 6 – Pressure coefficient determined by simulation and by experiment.

4. Conclusions

After analysis of velocity distribution will can seen that the velocity on upper surface is higher than the velocity on the lower surface.

The curves from Fig. 6 confirms a very good coincidence between simulation and experimental values of pressure coefficient around the profile, except the area of tailing edge where appear some difference.

The pressure coefficient of the airfoil's upper surface was negative and the lower surface was positive, thus the lift force of the airfoil is in the upward direction.

The CFD analysis, allows the user to study the aerodynamics of various geometries at different physical settings to get a true feel for how the specific profile might behave in real world applications.

CFD analysis is an efficient alternative to experimental methods because it is not conditioned by the existence of the physical model, measuring equipment and wind tunnel.

REFERENCES

Kandwal S., Singh S., *Computational Fluid Dynamics Study of Fluid Flow and Aerodynamic Forces on an Airfoil*, International Journal of Engineering Research & Technology (IJERT), Vol. **1**, ISSN: 2278-0181, 2012.

Kevadiya M., *CFD Analysis of Pressure Coefficient for NACA 4412*, International Journal of Engineering Trends and Technology, ISSN/EISSN: 22315381, Vol. **4**, 2041-2043, 2013.

Sagat C., Mane P., Gawali B.S., *Experimental and CFD Analysis of Airfoil at Low Reynolds Number*, International Journal of Mechanical Engineering and Robotics Research, Vol. **1**, No. *3*, 277-283, 2012.

Şahin I., Acir A., *Numerical and Experimental Investigations of Lift and Drag Performances of NACA 0015 Wind Turbine Airfoil*, International Journal of Materials, Mechanics and Manufacturing, Vol. **3**, No. *1*, 22-25, 2015.

ANALIZA CONTRASTIVĂ A CURGERII ÎN JURUL UNUI PROFIL

(Rezumat)

Scopul lucrării este de a determina prin analiză CFD, utilizând software-ul Ansys, distribuţia coeficientului de presiune în jurul unui profil plasat într-un jet de fluid. Dacă se cunoaşte distribuţia coeficientului de presiune se poate apoi determina forţa aerodinamică şi componentele sale: forţa de portanţă şi respectiv forţa de rezistenţă la înaintare. Viteza curentului de fluid este v = 50 m/s, densitatea aerului ρ = 1.16 kg/m^3, iar profilul are coarda c = 150 mm şi anvergura b = 110 mm, fiind poziţionat la un unghi de incidenţă α = 18º. În final rezultatele obţinute prin simulare sunt comparate cu cele experimentale măsurate în tunelul aerodinamic.

BULETINUL INSTITUTULUI POLITEHNIC DIN IAŞI
Publicat de
Universitatea Tehnică „Gheorghe Asachi” din Iaşi
Volumul 62 (66), Numărul 2, 2016
Secţia
CONSTRUCŢII DE MAŞINI

CFD ANALYSIS REGARDING THE INFLUENCE OF IMPELLER PARAMETERS ON THE PERFORMANCE OF A SIGLE-STAGE CENTRIFUGAL PUMP

BY

EUGEN-VLAD NĂSTASE*

“Gheorghe Asachi” Technical University of Iaşi,
Department of Fluid Mechanics, Fluid Machinery and Fluid Power Systems

Received: December 5, 2016
Accepted for publication: December 20, 2016

Abstract. The objective of the application is to determine, through Solid Works Flow Simulation, the influence of impeller parameters on the performance of a centrifugal pump. Rotor parameters whose influence on efficiency will be studied are: the shape blade geometry and number of blades respectively. For this purpose will design a pump impeller for working with a flow Q = 0.083 m^3/s, head H = 50 m, at a rotation speed n = 1450 rev/min. The rotor blades are constructed in three ways: simple arc method, double arc method, and point by point method. Also the number of blades will change to the value obtained by calculation, to see the influence of the number of blades on pump efficiency. For each type of rotor design, simulations will be made and tracked finding the optimal solution.

Keywords: centrifugal pump; flow simulation; turbo machinery; impeller design; computational fluid dynamics.

1. Introduction

Centrifugal pumps are widely used in many applications. This type of pump is used in various field such as in industries, agriculture and domestic

*Corresponding author; *e-mail*: nastase_eugenvlad@yahoo.com

applications. The input power of centrifugal pump is the mechanical energy, applied to the shaft, and the output energy is hydraulic energy of the fluid. Two main components of a centrifugal pump are the impeller and the casing (Fig. 1). The impeller is a rotating component and the casing is a stationary component. Water enters axially through the impeller eye and exits radially from impeller to casing in virtute of the centrifugal force produced by the impeller's speed. (Gundale and Joshi, 2013). The role of casing is to leads the liquid, from the impeller discharge to the outlet of pump and transform into pressure, a part of the kinetic energy of this fluid.

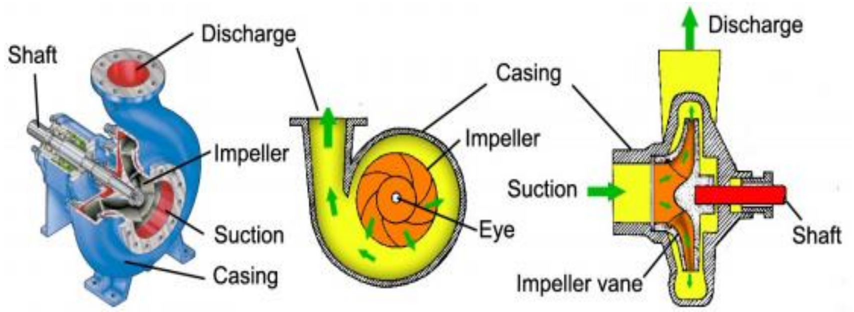

Fig. 1 – Centrifugal pump.

The impeller is a main part of a pump and the performance of this machine depends on the impeller diameters and design (shape of impeller vane). The impeller is a complex structure and the conventional method of verification is time consuming and expensive, the designer maybe used a CAD software in constructing the geometrical profile and CFD analysis for final model (Rajendran and Purushothaman, 2012).

2. Design of Impeller

General methods available to design an impeller vanes are simple arc method, double arc method, and point by point method (Gundale and Joshi, 2013; Wu *et al*., 2008). The main geometric parameters of impeller determined by classical methodology (Wu *et al*.,2008), are shown in Table 1.

Table 1
The Geometric Characteristics of Impeller

Pump head: H [m]	50	Outlet diameter : D_2 [mm]	400
Flow rate: Q [m^3/h]	300	Inlet blade angle: β_1[°]	17
Angular velocity: n [rad/s]	151.8	Outlet blade angle: β_2[°]	22
Specific speed: n_s	22.3	Blade inlet height: b_1 [mm]	40
Inlet diameter: D_1[mm]	175	Blade outlet height: b_2 [mm]	20

Number of rotor blades (z) were determined using Pfleiderer relationship (Budea and Carbune, 2012):

$$z = 6{,}5\,\frac{D_1 + D_2}{D_2 - D_1}\sin\frac{\beta_1 + \beta_2}{2} \tag{1}$$

With the parameters of impeller (Table 1) result for the number of blades z = 5.9. In conclusion, we consider for geometrical model and simulation, z = 5 and z = 6. Depending upon the calculated parameters the modelling of the impeller is done in Solid Works (three rotors with six blades and three rotors with seven blades) and then the CFD analysis is performed.

3. Results of Simulation

CFD analysis were carried out to predict the efficiency of impeller for the given input model. The efficiency is specified as a equation goal shown in next relation:

$$\eta = \frac{(P_{outlet} - P_{inlet})\cdot Q}{\omega\cdot M} \tag{2}$$

where, P_{inlet} is the pressure at the pump's inlet [Pa], P_{outlet} – the pressure at the impeller's outlet [Pa], Q – the volume flow rate [m^3/s], ω – angular velocity [rad/s], and M – the impeller torque [Nm].

Simulation results are presented as graphs of pressure distribution. In Figs. 2 and 3 we can see the distribution of pressure to the rotor built by the method of arc.

In Figs. 4 and 5 are shown distributions pressure to the rotor whose blades are constructed by double-arc method. In Figs. 6 and 7 can be observed the distribution of pressure for impeller with blades constructed using point by point method.

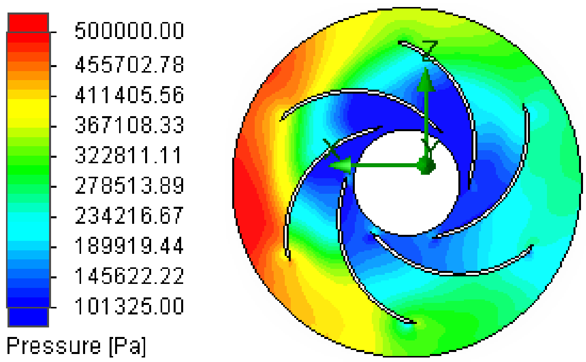

Fig. 2 – Contour of pressure (simple arc method, six blades).

Solid works flow simulation allows exporting the numerical results into Excel files. With data of Excel file was drawn chart efficiecy for all six impellers (Fig. 8).

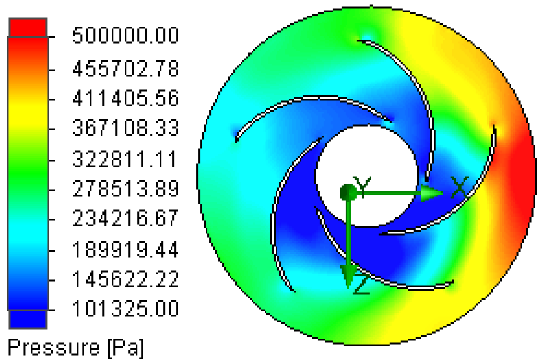

Fig. 3 – Contour of pressure (simple arc method, five blades).

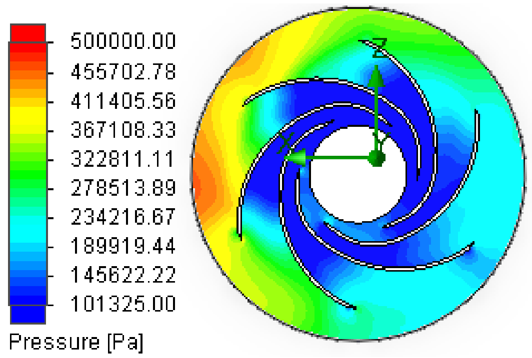

Fig. 4 – Contour of pressure (double arc method, six blades).

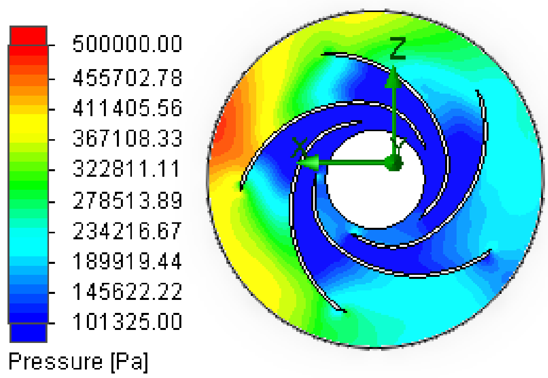

Fig. 5 – Contour of pressure (double arc method, five blade).

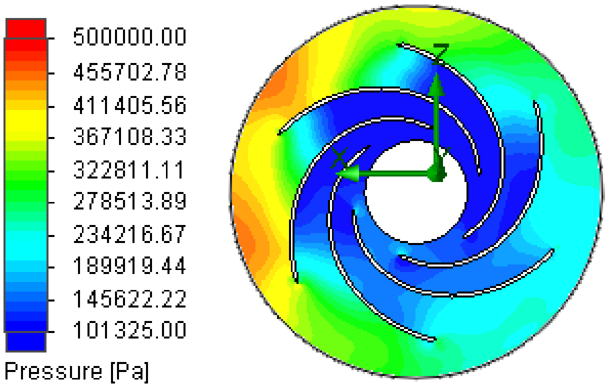

Fig. 6 – Contour of pressure (point by point method, six blade).

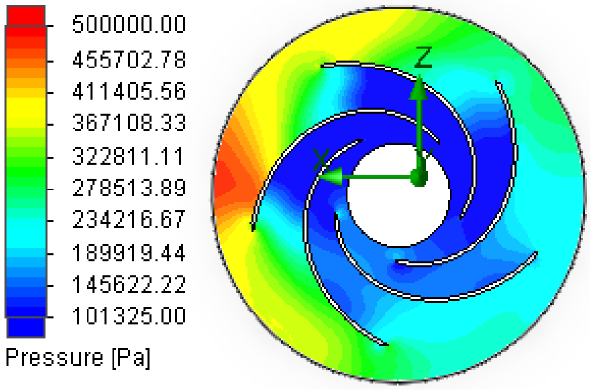

Fig. 7 – Contour of pressure (point by point method, five blades).

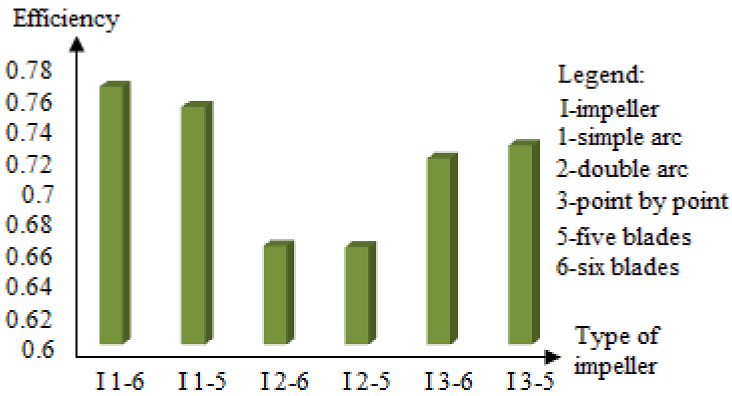

Fig. 8 – Efficiency chart for all impellers.

4. Conclusions

The pressure contours show a continuous pressure rise from leading edge to trailing edge of the impeller due to the dynamic head developed by the rotating pump impeller.

After analyzing the chart efficiency can be seen as the optimal variant is the impeller with six blades and blade profile built by the method of simple arc.

From the results obtained it is found that by decreasing the number of blades decreases and rotor's efficiency. For current conditions it is found that the optimum number is six blades.

CAD and CFD analysis are useful tools that reduce considerable time that is usually lost in physical testing.

REFERENCES

Budea S., Carbune V.D., *The Influence of the Inlet Angle Over the Radial Impeller Geometry Design Approach with Ansys*, Journal of Engineering Studies and Research, Vol. **18**, No. *4*, 32-39, 2012.

Gundale V.A., Joshi G.R., *A Simplified 3d Model Approach in Constructing the Plain Vane Profile of A Radial Type Submersible Pump Impeller*, Research Journal of Engineering Sciences, Vol. **2**, ISSN 2278 – 9472, 33-37, 2013.

Rajendran S., Purushothaman K., *Analysis of a Centrifugal Pump Impeller Using ANSYS-CFX*, International Journal of Engineering Research & Technology, Vol. **1**, ISSN: 2278-0181, 2012.

Wu K.,H., Lin B.J., Hung C.I., *Novel Design of Centrifugal Pump Impellers Using Generated Machining Method and CFD*, Engineering Applications of Computational Fluid Mechanics, Vol. **2**, No. *2*, 195-207, 2008.

ANALIZA CFD PRIVIND INFLUENȚA PARAMETRILOR ROTORULUI ASUPRA PERFORMANȚEI UNEI POMPE CENTRIFUGE MONOETAJATE

(Rezumat)

Scopul lucrării este de a determina, utilizând software-ul Solid Works Flow Simulation, influenţa parametrilor rotorului asupra randamentului unei pompe centrifuge. Parametrii rotorului care se vor studia, pentru a determina influența acestora asupra randamentului, sunt geometria paletei rotorului şi respectiv numărul de palete rotorice. În acest scop se va proiecta rotorul pentru o pompă centrifugă ce lucrează la un debit Q = 0,083 m^3/s, o sarcină H = 50 m şi o turaţie n = 1450 rot/min. Paletele rotorului vor fi construite prin trei metode: cu un arc de cerc, cu două arce de cerc şi respectiv prin puncte. De asemenea numărul de palete se vor modifica faţă de valoarea obţinută prin calcul, pentru a vedea influenţa numărului de palete asupra randamentului pompei. Pentru fiecare tip de rotor proiectat se fac simulări şi se compară randamentele obţinute.

BULETINUL INSTITUTULUI POLITEHNIC DIN IAŞI
Publicat de
Universitatea Tehnică „Gheorghe Asachi” din Iaşi
Volumul 62 (66), Numărul 2, 2016
Secţia
CONSTRUCŢII DE MAŞINI

EXPERIMNTAL INVESTIGATION OF THE INFLUENCE OF CUTTING EDGE REINFORCEMENT ON SPECIFIC CUTTING FORCE

BY

CRISTIAN CROITORU[*] and ANA-MARIA BOCĂNEŢ

"Gheorghe Asachi" Technical University of Iaşi,
Faculty of Machine Manufacturing and Industrial Management

Received: December 6, 2016
Accepted for publication: December 28, 2016

Abstract. This paper presents an investigation on the influence of cutting edge preparation represented by edge chamfering on cutting efforts. Turning of steel 31MnCrSi11/STAS 791 (60 CrMo3/AFNOR NF) with variable design cemented carbide inserts was performed, cutting forces were measured and values of specific cutting force k_c and unit specific cutting force $k_{c1.1}$ were computed.

Keywords: chamfered edge; specific cutting force; dry machining.

1. Introduction

As it is well known, reinforcement of the cutting edge of cutting tools aims to increase its resistance to bending and to shocks produced especially during roughing operations (Stephenson and Agapiou, 1996, Chen *et al.* 2005).

A common way of reinforcing the cutting edge is to achieve a chamfer defined by an angle γ_f (usually having negative values) and a width f_γ (Fig. 1). The positive effect of the increased resistance of the cutting edge is

[*]Corresponding author; *e-mail*: ccroitoru2003@yahoo.com

accompanied by negative effect of increased tangential force F_c as is presented in Fig. 2 (Stahl and de Vos, 2014; Kurt and Şeker, 2005).

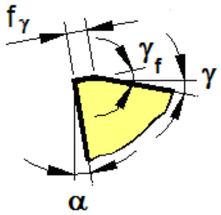

Fig. 1 – Chamfered edge characterization.

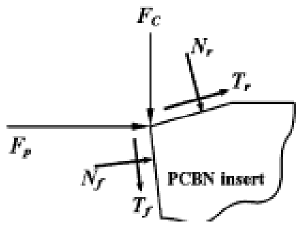

Fig. 2 – Effect of chamfered edge on the load insert.

Influence of chamfer cutting edge on chips formation depends on the ratio in which the chip thickness h and the width of facet f_γ are found, as follows (Sandvik Coromant, 2010):

– when h is smaller than f_γ ($h < f_\gamma$), the facet takes the role of rake face, and the chip is formed similar to case of $\gamma = \gamma_f$ and $f_\gamma = 0$ (Fig. 3);

– when h is greater than f_γ ($h > f_\gamma$) the tangential component of the cutting force F_c is rising.

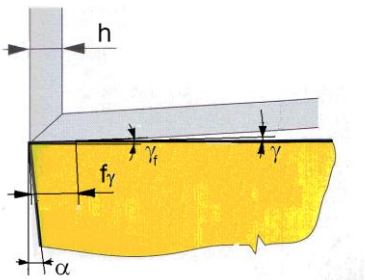

Fig. 3 – Influence of chamfer cutting edge on chips formation.

The influence of the rake value γ on the cutting force is also known. The cutting effort increases when this angle decreases (Shaw, 1997; Günaya *et al*., 2005).

In this study, the influence of edge chamfer width on main cutting force was determined during machining of 31MnCrSi11/STAS 791 (60 CrMo3/AFNOR NF) steel with different values of undeformed chip thickness. As a result of experimental evaluation, the values of specific cutting force k_c and unit specific cutting force $k_{c1.1}$ were calculated.

2. Materials and Methods

Experimental tests were carried out on a cylindrical steel blank 31MnCrSi11/STAS 791 (60 CrMo3/AFNOR NF) having the properties shown below.

Chemical composition [%]		
C	0.34	
Si	1.09	
Mn	0.844	
Cr	1.10	
Mechanical properties		
Hardness (Brinell)		250
Yield strength STAS 791 value [MPa]		830

Fig. 4 – Chemical composition and mechanical properties of experimental samples.

Experiments were carried out on a conventional lathe SNA 560x1500 in dry cutting condition by considering the parameters presented in Fig. 5.

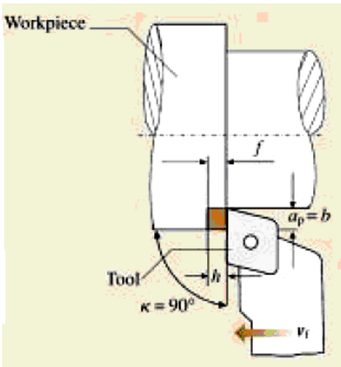

Fig. 5 – Cut and chip variables.

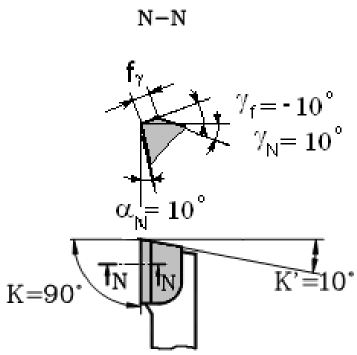

Fig. 6 – Geometric features of the utilized cutting tool.

a *b*

Fig. 7 – Cutting tool: *a* – sharp edge cutting tool; *b* – chamfered edge cutting tool.

Machining tests were conducted by using uncoated carbide P20 tools inserts having different reinforcement as is presented in Figs. 6 and 7.

The others geometric parameters of the considered cutting tools were (Fig. 6).

- major cutting angle K = 90°;
- minor cutting angle K' = 10°;
- nose radius R < 0.05 mm;
- inclination angle λ = 0°;
- clearance angle α_N = 10°;
- cutting edge roundness r < 0.02 mm;
- rake angle γ_N = 10°.

A piezoelectric dynamometer Kistler 9272 was used to measure the main component force during the experiments.

Specific cutting force was determined by the graphic-analytical method set out above (Croitoru *et al*., 2015).

3. Results and Discussion

Three sets of experiments were performed in random order, considering three values of facet of chamfered edge f_γ, according to Table 1.

Table 1
Measured Average Values of Components of the Cutting (Main) Force

No. test	f [mm/rot]	Cutting conditions	F_z (F_c) med. value [N]
1.	0.05	γ = +10°; K = 90°; V_c = 75 m/min; a_p = 2 mm; f_γ = 0 mm	326
2.	0.10		540
3.	0.20		972
4.	0.31		1433
5.	0.05	γ = +10°; K = 90°; V_c = 60.47 m/min; a_p = 2 mm; f_γ = 0.12 mm	362
6.	0.10		574
7.	0.20		909
8.	0.31		1458
9.	0.05	γ = +10°; K = 90°; V_c = 68 m/min; a_p = 2 mm; f_γ = 0.4 mm	486
10.	0.10		670
11.	0.20		963
12.	0.31		1392

The first set of experiments (1-4) was performed with the tool having sharp edge (Fig. 7*a*). Values of feed f characteristic of both finishing and roughing operations were considered.

The second set of experiments was carried out with the tool having 0.12 mm width of facet f_γ of the chamfer (Figs. 6 and 7*b*). The feed values *f* were selected so that both the case of chip thickness *h* is less than the width facet f_γ ($h < f_\gamma$) and when is higher than this ($h > f_\gamma$) was considered (Figs. 3 and 6).

The third set of experiments (9-12) aimed to highlighting the manner in which the specific cutting force is influenced by the low values of the rake angle γ. For this reason, the feed values *f* are aimed to achieve the condition that the chip thickness *h* is smaller than the width of facet f_γ ($h < f_\gamma$).

Since the sets of experiments 2 and 3 fulfill the condition $h < f_\gamma$, may be considered that, by these experiments, it can be studied the influence of rake angle on the cutting effort.

3.1. General Evaluation

Using the data presented in Table 2, graphs of evolution of the main component of cutting force F_c (F_z) were plotted by considering its average values recorded for each experiment presented in Fig. 8.

As expected, in all three cases were recorded increases of component F_c with the feed *f* or with the undeformed chip thickness *h*.

The highest rate of increasing of force F_c depending the feed *f* was recorded for the sharp edge ($f_\gamma = 0$), and the lowest for $f_\gamma = 0.4$ mm.

Comparing sets of experiments 2 and 3 may be inferred the rake angle influence on component F_c: F_c component increases when the rake angle γ decreases, a fact reported by Günaya *et al.* (2005), in case of steel turning with PCBN inserts.

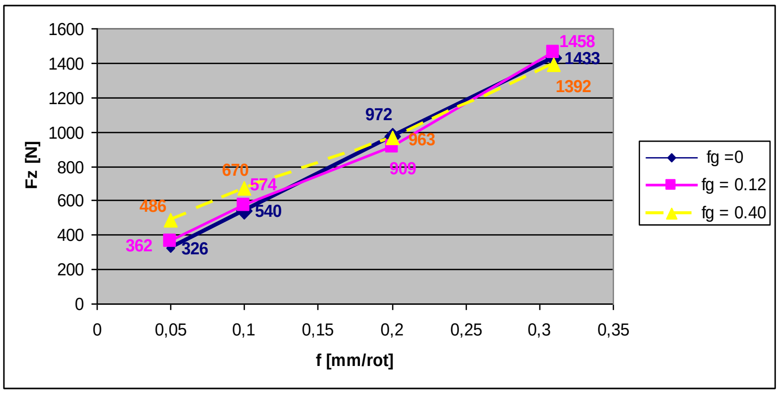

Fig. 8 – Evolution of cutting force *Fc* (F_z) depending on negative facet values for different feed rates.

A facet $f\gamma$ having 0.12 mm leads to a slight increase (about 10%) of the component F_c in the case where the chip thickness is smaller than the width of the chamfer ($h < f\gamma$).

If the thickness h is greater than the width chamfer $f\gamma$ ($h > f\gamma$) the F_c component is increasing, the rate of growing is somewhat less than the sharp edge case ($f\gamma = 0$).

This observation can be useful in finishing operations when cutting force value should be minimized.

3.2. Evaluation of Influence of Cutting Edge Reinforcement on Specific Cutting Force

The Kienzle equation of the main cutting force is:

$$F_c = k_c \cdot A = k_c \cdot h \cdot b = k_{c1.1} \cdot b \cdot h^{1-m_c} \quad (1)$$

where: k_c is the specific cutting force; $k_{c1.1}$ – the unit specific cutting force; b – the theoretical chip width (Fig. 5); h – the theoretical chip thickness; A – the theoretical chip area; m_c – the exponent of the specific cutting force.

Following the methodology used by (Croitoru *et al.*, 2015), for the three sets of experiments were calculated necessary data by using the values presented in Table 2. The graphs from Figs. 9, 10 and 11 were then plotted.

These charts represent the interpolation line of the Eq. (2) computed for each set of tests:

$$\lg \frac{F_c}{b} = \lg k_{c1.1} + (1 - m_c) \cdot \lg h \quad (2)$$

Table 2
Considered Values of Eq. (2)

No. test	f [mm/rot]	F_c [N]	F_c/b [N/m]	lg$f$	$\lg \frac{F_c}{b^*}$
1.	0.05	326	163	- 1.301	2.2121
2.	0.10	540	270	- 1.0	2.4313
3.	0.20	972	486	- 0.6989	2.6866
4.	0.31	1433	716.5	- 0.5086	2.8552
5.	0.05	362	181	- 1.301	2.2576
6.	0.10	574	287	- 1.0	2.4579
7.	0.20	909	454.5	- 0.6989	2.6575
8.	0.31	1458	729	- 0.5086	2.8627
9.	0.05	486	243	- 1.301	2.3856
10.	0.10	670	335	- 1.0	2.5250
11.	0.20	963	481.5	- 0.6989	2.6826
12.	0.31	1392	696	- 0.5086	2.8426

*$b = a_p = 2$ mm, according to experimental plan

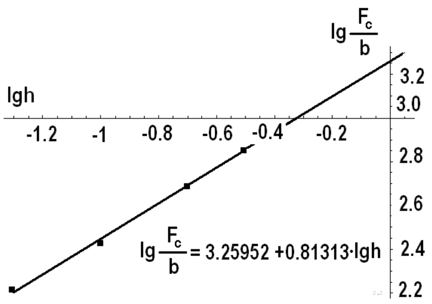

Fig. 9 – Plot of 1st set of experimental data in logarithmic coordinates.

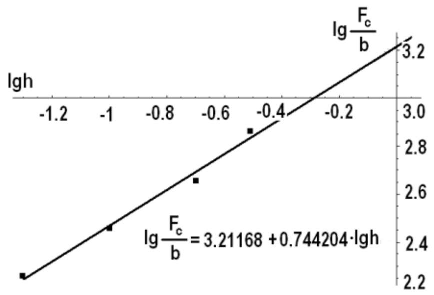

Fig. 10 – Plot of 2nd set of experimental data in logarithmic coordinates.

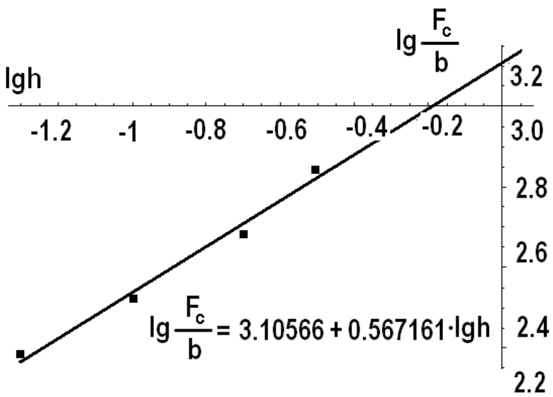

Fig. 11 – Plot of 3rd set of experimental data in logarithmic coordinates.

Table 3
Calculated Values for the Coefficients $k_{c1.1}$ and m_c

	set 1 $f\gamma = 0$ [mm]	set 2 $f\gamma = 0.12$ [mm]	set 3 $f\gamma = 0.12$ [mm]
$k_{c1.1}$ [N]	1816	1628	1275
m_c	0.18687	0.25579	0.43283

By using the relations shown in Figs. 9, 10 and 11, the values of the constants $k_{c1.1}$ and m_c shown in Table 3 were calculated.

Finally, the Eq. (1) and the data from Table 3 were used to calculate the specific cutting force values listed in Table 4.

Table 4

Computed Values of Equation Specific Cutting Force k_c

No. test	f [mm/rot]	f_γ [mm]	k_c [N]
1.	0.05	0	3178
2.	0.10		2792
3.	0.20		2453
4.	0.31		2260
5.	0.05	0.12	3503
6.	0.10		2933
7.	0.20		2457
8.	0.31		2196
9.	0.05	0.40	4662
10.	0.10		3454
11.	0.20		2559
12.	0.31		2117

The specific cutting force values from Table 4 analyze leads to the following observations:

For all three sets of experiments, the increase of feed rate f (equivalent to increasing the thickness h of the chip) led to lower specific cutting force, thus confirming the information known from the literature (Klocke, 2011);

Comparing the corresponding values of sets 1 (tests 1-4) and 2 (tests 5-8) leads to the observation that, if the chip thickness is smaller than the width of chamfer ($h < f\gamma$), there is a slight increase in the specific cutting force value k_c (less than 10%); if the thickness of h values continue to increase over the value of the facet f_γ, the k_c values decrease to give lower values than those calculated in case of sharp edge tool;

The sharp decreasing of the rake angle (tests 9-12) leads to the increasing of the value of k_c; when increasing thickness values h, appears the same trend as in the 2nd set, that is of decreasing of the difference compared to the k_c values reported for the sharp tool;

The use of cutting chamfered cutting edges leads to decreasing of values of specific cutting unit $k_{c1.1}$ and increasing of coefficient m_c values from Eq. (1); it can be concluded that, in case of chamfered cutting edges, increases the influence of chip thickness h (feed f) on specific cutting force and therefore of F_c component;

Considering the same working conditions, changing the cutting edge preparation can lead to a significant change of value of specific cutting unit $k_{c1.1}$; thereby are confirmed the general recommendation not to use this parameter as a criterion of machinability (Toenshoff and Denkena, 2013).

4. Conclusions

The aim of this study was to investigate the effects of cutting edge preparation on cutting forces. The cutting forces were measured in turning of a 60 CrMo3/AFNOR NF steel and were determined the values of specific cutting force and also its specific coefficients $k_{c1.1}$ and m_c. The effects of the feedrates and of the facet of chamfered edge were evaluated.

With reference to the results, the following conclusions can be drawn:

• Using a chamfered cutting edge significantly modify cutting forces and therefore specific cutting force and its coefficients;

• The influence of chamfered cutting edge on the magnitude of cutting force depends on the ratio between chip thickness h (feed rate f) and chamfer width f_γ;

• It was obvious that, for a certain ratio of chip thickness h and width facet f_γ , the cutting efforts start decreasing; this can be useful when cutting force must be minimized;

• When using a chamfered edge increases the influence of feed rate f on the magnitude of cutting forces and therefore of specific cutting force.

REFERENCES

Chen L., El-Wardany T., Nasr M., Elbestawi M.A., *Effects of Edge Preparation and Feed when Hard Turning a Hot Work Die Steel with Polycrystalline Cubic Boron Nitride Tools*, Annals of the CIRP Vol. 55/1/2006.

Croitoru C., Bocăneţ A.-M., Chelariu R., Chicet D., *Evaluation of Machinability of AlCu11 Cast Alloy at Conventional Cutting Speeds*, Bul. Inst. Polit. Iaşi, **LXI (LXV)**, *2*, s. Construcţii de Maşini, 131-142, ISSN 1011-2855 (2015).

Günaya M., Korkut I., Aslan E., Şeker U., *Experimental Investigation of the Effect of Cutting Tool Rake Angle on Main Cutting Force*, Journal of Materials Processing Technology, **166**, 44-49, ISSN 0924-0136 (2005).

Klocke F., *Manufacturing Processes 1: Cutting*, Springer-Verlag Berlin Heidelberg 2011, ISSN 1865-0899, ISBN 978-3-642-11979-8.

Kurt A., Şeker U., *The Effect of Chamfer Angle of Polycrystalline Cubic Boron Nitride Cutting Tool on the Cutting Forces and the Tool Stresses in Finishing Hard Turning of AISI 52100 Steel*, Materials and Design, **26**, 351-356, ISSN 0264-1275 (2005).

Shaw M.C., *Metal Cutting Principles*, Oxford University Press Inc., New York, 1997, ISBN 0-19-859020-2.

Stahl J.-E., de Vos P., *Metal Cutting Theories in Practice*, SECO TOOLS AB, Lund-Fagersta, Sweden 2014, 02980331, ST20146464 GB, Version 1.1.

Stephenson D.A., Agapiou J.S., *Metal Cutting Theory and Practice*, Marcel Dekker, New York 1996, ISBN 0824795792.

Toenshoff H.K., Denkena B., *Basics of Cutting and Abrasive Processes*, Springer-Verlag Berlin Heidelberg 2013, ISSN 2194-0525, ISBN 978-3-642-33256-2.

* * * *Metal Cutting Technology, Technical Guide*, C-2900:7, ENG/01 © AB Sandvik Coromant, 2010.

CERCETĂRI EXPERIMENTALE PRIVIND
INFLUENŢA RANFORSĂRII TĂIŞULUI SCULEI ASUPRA
FORŢEI SPECIFICE DE AŞCHIERE

(Rezumat)

Microgeometria tăişului unei scule aşchietoare reprezintă un instrument eficient în optimizarea constructiv-funcţională a acesteia.

Eficienţa acestui instrument poate fi dedusă şi prin constatarea marii diversităţi de tipuri şi dimensiuni pe care o oferă firmele producătoare de scule. În ciuda faptului că modificarea microgeometriei tăişului este foarte răspândită la sculele moderne, există puţine informaţii cantitative privind influenţa pe care aceasta o are asupra eforturilor de aşchiere.

Lucrarea de faţă prezintă o modalitate de evaluare a influenţei pe care o manifestă unul dintre parametrii microgeometriei tăişului asupra eforturilor de aşchiere, respectiv asupra forţei specifice de aşchiere.

BULETINUL INSTITUTULUI POLITEHNIC DIN IAŞI
Publicat de
Universitatea Tehnică „Gheorghe Asachi” din Iaşi
Volumul 62 (66), Numărul 2, 2016
Secţia
CONSTRUCŢII DE MAŞINI

EXPERIMENTAL CHARACTERIZATION OF MATERIALS SUBJECTED TO COMBINED LOADINGS PART II: TORSION-TENSION

BY

LIVIU ANDRUŞCĂ*

"Gheorghe Asachi" Technical University of Iaşi,
Department of Mechanical Engineering, Mechatronics and Robotics

Received: June 22, 2016
Accepted for publication: December 19, 2016

Abstract. Combined torsion-axial loading is an experimental procedure that provides information about the elasto-plastic behavior and failure mechanisms of materials. When different values of twist angles are achieved, torsion initial loading of circular specimens is stopped. Subsequently tensile loads are applied until break. Hardness and Young's modulus are determined by instrumented indentation test. These two parameters together with material microstructure changes depends on the ratio between the two types of loadings. Material failure is governed by different mechanisms and is influenced either by predominant action of normal stresses/shear stresses.

Keywords: mechanical testing; combined loadings; SEM analysis; nanoindentation tests; materials failure.

1. Introduction

Investigation of materials behavior subjected to complex loadings presents a major practical interest and is a difficult task. The experimental set-ups developed for performing multiaxial loading tests are very varied. Combined torsion-axial loading can be conducted in static or dynamic

*Corresponding author; *e-mail*: liviu.andrusca@tuiasi.ro

conditions, with tubular or cylindrical specimens. The aims of such researches are to investigate material mechanical behavior, to characterize failure modes, to define adequate constitutive models, etc. Combined loading through torsion and tensile tests is an experimental technique that can be applied to a wide range of materials: steel (Andrușcă *et al.*, 2015; Andrușcă, 2016a; Andrușcă *et al.*, 2016b), pure copper (Li *et al.*, 2014; Wang *et al.*, 2013), polymers (Guitton *et al.*, 2014), composites (Wang *et al.*, 2014) etc. For some metallic materials, through torsion test, large plastic deformations are applied without any change in the sample's shape and size (Guo *et al.*, 2016). Depending on the stress state can be observed different ductile rupture mechanisms that can be identified by a micromechanical study using scanning electron microscopy of the fractured surfaces (Barsoum and Faleskog, 2007). Getting information from nano-indentation experiments (Clausner *et al.*, 2014) or by determining Vickers hardness (Zhang *et al.*, 2011), can be established correlations between different mechanical properties materials and hardness.

2. Material and Methods

Combined torsion and axial loadings have assumed three stages to test circular section specimens made from S 235 JR structural steel: 1) torsion preloading, 2) elastic discharge, 3) tensile reloading until break (Fig. 1).

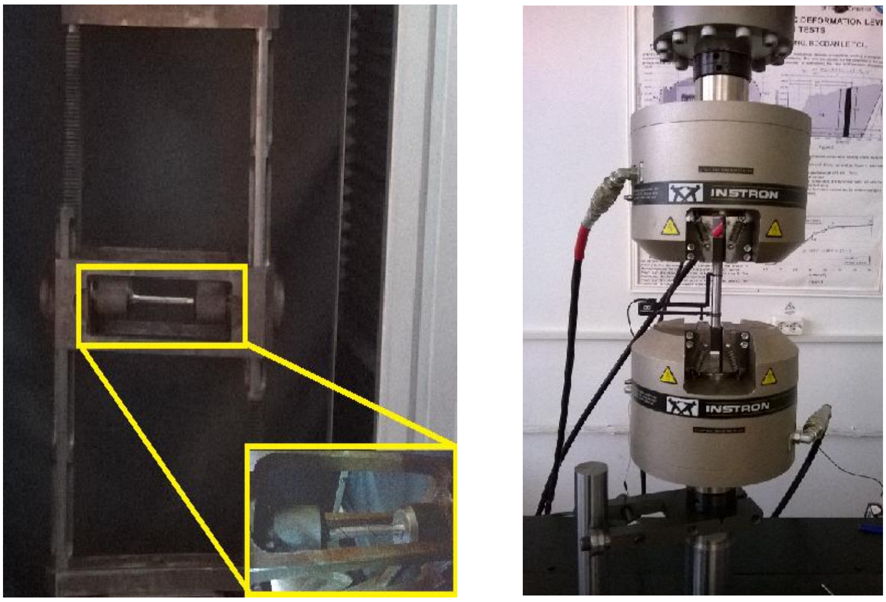

a *b*

Fig. 1 – Combined loading of specimens with circular cross section:
a – torsion test; *b* – tensile test.

Successive loadings were initiated with torsion tests followed by tensile tests. Torsion tests are performed on a universal testing machine WDW 50 using an attachable device that allows axial displacements of specimens. Pretorsion implied loading specimens with different values of rotation angle. Subsequent tensile tests were conducted on an Instron 8801 Servohydraulic Fatigue Testing System. Reloading of specimens by tensile testing, was made up to breaking. After specimens are broken disc samples have been cut out and they have been subjected to instrumented indentation test. Also, rupture surfaces are investigated to evaluate microstructural changes and failure modes.

3. Results and Discussions

To investigate the material behavior and failure mode, circular specimens fabricated from S 235 JR are subjected to combined torsion-axial loading. When imposed value of twist angle is reached initial test is stopped. The experiment continues with tensile test, with different values of extensions depending on when specimens break. Twist angle and extension values for each specimen are presented in Table 1.

Table 1

Values of Twist Angle and Extension for the Six Specimens

Test parameters	Sample no.					
	S_1	S_2	S_3	S_4	S_5	S_6
φ [°]	1279.55	1031.23	782.94	534.63	286.31	37.99
Δl [mm]	16.83	19.46	16.79	20.96	22	24.4

In Fig. 2 are presented the equipment used for instrumented indentation tests and load-depth curve used to determine H_{IT} and E_{IT}.

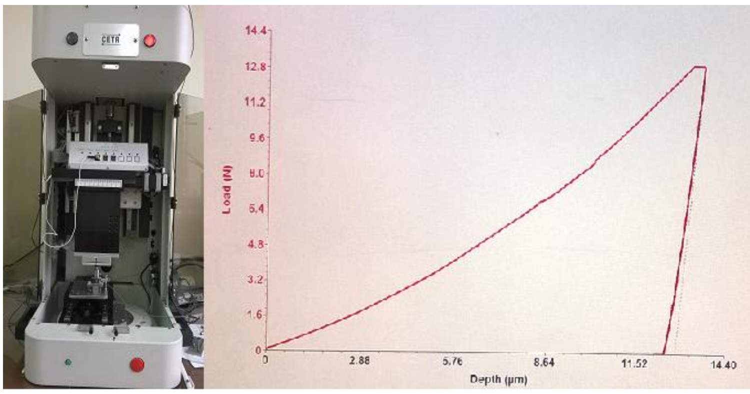

Fig. 2 – Equipment used in nanoindentation tests and load-depth resultant curve.

Fracture surfaces corresponding to four different specimens S_1, S_2, S_4 and S_6 are illustrated in Fig. 3.

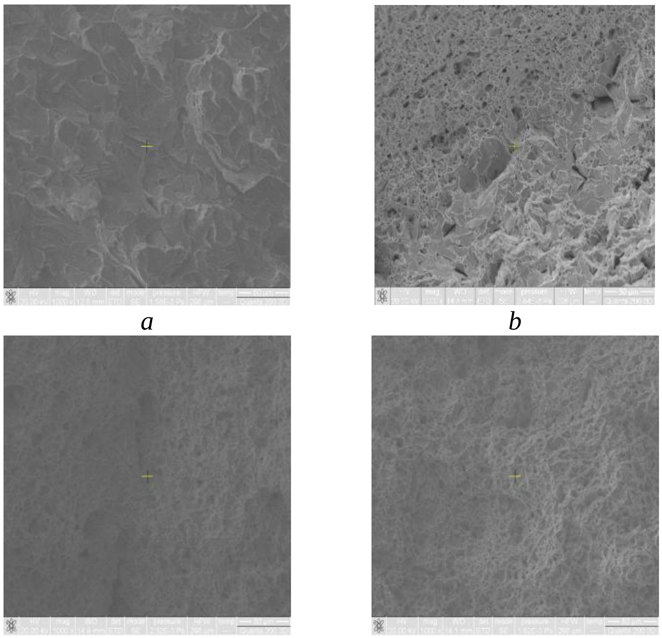

a *b* *c* *d*

Fig. 3 – SEM fractographs showing the failure modes for S 235 JR:
(*a*) S_1; (*b*) S_2; (*c*) S_4; (*d*) S_6 (magnitude *1000X*).

It was made an average of measured values for each sample to illustrate instrumented hardness and Young's modulus variation. Young's modulus variation is presented in Fig. 4.

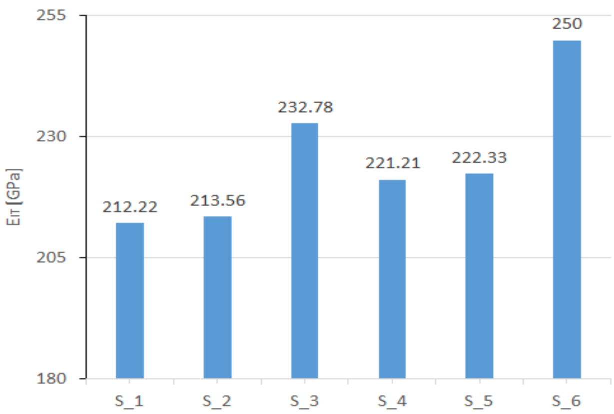

Fig. 4 – Young's modulus variation after torsion-tensile combined loading.

In the case of sample S_1 (φ = 1279.55°) it was found the minimum value of Young's modulus (212.22 GPa). The maximum value was obtained for sample S_1 (φ = 37.99°).

Variation of hardness for the six samples is presented in Fig. 5.

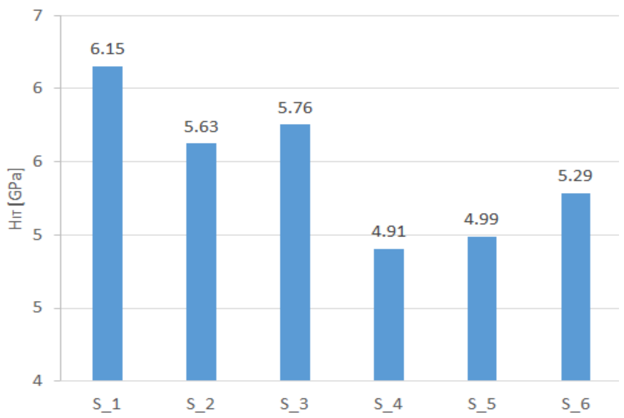

Fig. 5 – Hardness variation after torsion-tensile combined loading.

The higher value of indentation hardness (6.15 GPa) is found for specimen S_1, which has been tested with maximum value of rotational angle. The minimum hardness value is recorded for specimen S_3 (4.91 GPa) which is not the sample with smallest value of twist angle.

4. Conclusions

The present work shows the influence of combined torsion-axial loading on material parameters such as hardness and Young modulus and on failure mechanisms. Young's modulus increases with decreasing of twist angle for specimens subjected to initial torsion and subsequent tensile tests, while hardness presents a decreasing trend. This changes are due to material hardening by initial torsion and subsequent tensile. Study of resulting fracture surfaces showed that material failure occurred in most cases due to tensile load.

REFERENCES

Andruşcă L., Goanţă V., Bârsănescu P.D., Istrate B., *Investigation of Materials Behavior under Combined Loading Conditions*, Bul. Inst. Polit. Iasi, **LXI (LXV)**, *2*, s. Construcţii de Maşini, 23-28 (2015).

Andruşcă L., *Experimental Characterization of Materials Subjected to Combined Loadings: Part I: Tension-Torsion*, Bul. Inst. Polit. Iaşi, **62 (66)**, *1*, s. Construcţii de Maşini, 93-98 (2016a).

Andruşcă L., Goanță V., Bârsănescu P.D., Savin A., *Experimental Characterization of Materials Subjected to Combined Loading Conditions*, IOP Conference Series, Materials Science and Engineering, ACME2016, Iași (2016b*).*

Barsoum I., Faleskog J., *Rupture Mechanisms in Combined Tension and Shear - Experiments*, Int. Journal of Solids and Structures, **44**, 1768-1786 (2007).

Clausner A., Richter F., *Determination of Yield Stress from Nano-Indentation Experiments*, European Journal of Mechanics A/Solids, **51**, 11-20 (2015).

Guitton E., Rio G., Laurent H., *A New Multiaxial Loading Test for Investigating the Mechanical Behavior of Polymers*, Polymer Testing, **36**, 32–43 (2014).

Guo N., Song B., Yu H., Xin R., Wang B., Liu T., *Enhancing Tensile Strength of Cu by Introducing Gradient Microstructures via a Simple Torsion Deformation,* Materials and Design, **90**, 545-550 (2016).

Li J., Li F., Hussain M., Wang C., Wang L., *Micro-Structural Evolution Subjected to Combined Tension–Torsion Deformation for Pure Copper*, Materials Science & Engineering A, **610**, 181-187 (2014).

Wang C., Li F., Wei L., Yang Y., Dong J., *Experimental Microindentation of Pure Copper Subjected to Severe Plastic Deformation by Combined Tension–Torsion*, Materials Science and Engineering A, **571**, 95-102 (2013).

Wang D., Wu M.S., *Poynting and Axial Force–Twist Effects in Nonlinear Elastic mono- and bi-Layered Cylinders: Torsion, Axial and Combined Loadings*, International Journal of Solids and Structures, **51**, 1003-1019 (2014).

Zhang P., Li S.X., Zhang Z.F., *General Relationship between Strength and Hardness*, Materials Science and Engineering A, **529**, 62-73 (2011).

CARACTERIZAREA EXPERIMENTALĂ A MATERIALELOR SUPUSE LA SOLICITĂRI COMBINATE PARTEA A II-A: TORSIUNE CU TRACŢIUNE

(Rezumat)

Solicitarea combinată a organelor de mașini și a elementelor structurale este frecvent întâlnită în aplicațiile inginerești. Cunoașterea comportamentului și a modului de cedare a materialelor cu un istoric complex al încărcărilor și deformațiilor este de o importanță capitală. Solicitarea combinată la torsiune cu tracțiune a epruvetelor cu secțiune circulară oferă informații despre comportamentul la deformații plastice mari și despre cedarea materialelor solicitate inițial în domeniul elasto-plastic, descărcate elastic și solicitate ulterior până la rupere. În funcție de gradul de încărcare aplicat, prin cele două solicitări (inițială și finală), se poate observa că unele proprietăți mecanice ale materialului suferă modificări. Duritatea și modulul de elasticitate longitudinală, determinate prin teste de nanoindentare, variază ca urmare a ecruisării materialului. Totodată cedarea variază de la un mecanism influențat predominant de tensiunile tangențiale la un mecanism în care influența dominantă o au tensiunile normale. Prin modificarea raportului solicitărilor s-a constatat că există o tranziție între cele două mecanisme de cedare.